J. Fluid Mech. (2008), *vol.* 603, *pp.* 63–100.
doi:10.1017/S0022112008000797 Printed in the United Kingdom

Evolution of clusters of sedimenting low-Reynolds-number particles with Oseen interactions

G. SUBRAMANIAN[1] AND DONALD L. KOCH[2]

[1]Engineering Mechanics Unit, Jawaharlal Nehru Centre for Advanced Scientific Research, Jakkur, Bangalore, 560064, India

[2]School of Chemical and Biomolecular Engineering, Cornell University, Ithaca, NY 14853, USA

(Received 29 January 2007 and in revised form 21 January 2008)

A theoretical framework is developed to describe, in the limit of small but finite Re, the evolution of dilute clusters of sedimenting particles. Here, $Re = aU/\nu$ is the particle Reynolds number, where a is the radius of the spherical particle, U its settling velocity, and ν the kinematic viscosity of the suspending fluid. The theory assumes the disturbance velocity field at sufficiently large distances from a sedimenting particle, even at small Re, to possess the familiar source–sink character; that is, the momentum defect brought in via a narrow wake behind the particle is convected radially outwards in the remaining directions. It is then argued that for spherical clusters with sufficiently many particles, specifically with N much greater than $O(R_0U/\nu)$, the initial evolution is strongly influenced by wake-mediated interactions; here, N is the total number of particles, and R_0 is the initial cluster radius. As a result, the cluster first evolves into a nearly planar configuration with an asymptotically small aspect ratio of $O(R_0U/N\nu)$, the plane of the cluster being perpendicular to the direction of gravity; subsequent expansion occurs with an unchanged aspect ratio. For relatively sparse clusters with N smaller than $O(R_0U/\nu)$, the probability of wake interactions remains negligible, and the cluster expands while retaining its spherical shape. The long-time expansion in the former case, and that for all times in the latter case, is driven by disturbance velocity fields produced by the particles outside their wakes. The resulting interactions between particles are therefore mutually repulsive with forces that obey an inverse-square law. The analysis presented describes cluster evolution in this regime. A continuum representation is adopted with the clusters being characterized by a number density field ($n(\boldsymbol{r}, t)$), and a corresponding induced velocity field ($\boldsymbol{u}(\boldsymbol{r}, t)$) arising on account of interactions. For both planar axisymmetric clusters and spherical clusters with radial symmetry, the evolution equation admits a similarity solution; either cluster expands self-similarly for long times. The number density profiles at different times are functions of a similarity variable $\eta = (r/t^{1/3})$, r being the radial distance away from the cluster centre, and t the time. The radius of the expanding cluster is found to be of the form $R_{cl}(t) = A(\nu a)^{1/3}N^{1/3}t^{1/3}$, where the constant of proportionality, A, is determined from an analytical solution of the evolution equation; one finds $A = 1.743$ and 1.651 for planar and spherical clusters, respectively. The number density profile in a planar axisymmetric cluster is also obtained numerically as a solution of the initial value problem for a canonical (Gaussian) initial condition. The numerical results compare well with theoretical predictions, and demonstrate the asymptotic stability of the similarity solution in two dimensions for long times, at least for axisymmetric initial conditions.

1. Introduction

In this paper, the evolution of clusters of sedimenting spherical particles, on account of hydrodynamic interactions, is examined analytically when the particle Reynolds number, Re, is no longer identically zero. The Reynolds number is a dimensionless measure of the importance of inertial effects at the micro (particle)-scale, and is defined as $Re = aU/\nu$; here a is the particle radius, U a characteristic velocity scale, and ν the kinematic viscosity of the suspending fluid. Understanding the behaviour of such inertial clusters is relevant to the dynamics of particulate gravity currents and pyroclastic flows, and thence to the dispersion of pollutants and toxins. For instance, the dynamics of particulate gravity currents, turbidity currents in oceanic basins for example, is usually dominated by inertial and buoyancy forces, the latter arising because the suspended particles are heavier than the ambient fluid. The buoyancy forces that drive the current therefore evolve with time owing to the changing concentration of particles. Typical models make the diluteness assumption, neglecting interparticle hydrodynamic interactions. In addition, particles are assumed to settle out of suspension at a rate given by their terminal settling velocity in the absence of micro-scale inertia (see Hogg, Ungarish & Huppert 2001; Hogg, Hallworth & Huppert 2005). Other potential industrial applications of this study include mixing and combustion, bio-reactors, explosive ejecta etc., since, in many of these cases, particle motion is dominated by inertial forces. Hydrodynamic interactions between particles have been studied extensively in the quasi-steady inertialess limit ($Re = 0$), both specifically in the context of cluster evolution, and otherwise (for instance, see Happel & Brenner 1965; Kim & Karrila 1991; Brady & Bossis 1988); there has been limited progress, however, in analysing more complicated scenarios prevalent at finite Re.

In our study, we assume Re to be small but finite, where U in the definition of Re may now be taken as the single-particle settling velocity in a quiescent fluid. In the interests of analytical tractability, the cluster is assumed to be dilute; more precisely, the interparticle separation is much greater than the inertial screening length ($\nu/U = aRe^{-1}$ for $Re \ll 1$). The latter is the length scale at which convection of momentum becomes comparable to viscous diffusion, and changes the rate of decay of the disturbance velocity field. The above assumption simplifies the algebraic form of the inertial interactions, while still retaining the basic physics, and allows a quasi-steady evolution of the cluster even at finite Re. As originally shown by Oseen (see Batchelor (1967)), the simplified velocity field at large distances comprises an $O(1/r^2)$ irrotational source flow everywhere, r being the distance from the particle, except in a narrow wake behind the particle, where viscous effects remain significant; here, the velocity disturbance continues to decay as $1/r$, leading to a viscous drag on the particle.

Further, the detailed analysis is restricted to clusters where the probability of wake-mediated interactions between particles remains asymptotically small. Physical arguments show that, for initially spherical clusters with radii smaller than $O(N\nu/U)$ (N being the number of particles comprising the cluster), the above restriction implies that the analysis becomes valid only after an initial period during which the cluster evolves towards a nearly planar configuration primarily on account of wake-mediated interactions. Spherical clusters with radii larger than $O(N\nu/U)$, on the other hand, are unaffected by wake interactions, and expand without deformation. Thus, the analysis offers a quantitative description of evolving spherical and planar clusters in the limit where the inertial interaction fields within the sedimenting cluster are isotropic and repulsive. These simplifications, whose physical significance is discussed in more detail

below, enable one to rigorously examine the effects of fluid inertia on cluster evolution in a simpler setting. This should then serve as a first step in the quantitative study of general three-dimensional particle clusters at finite Re.

Earlier studies of the effects of hydrodynamic interactions on the dynamics of sedimenting clusters have been carried out in the absence of inertia, for instance, those of Nitsche & Batchelor (1997) and Machu *et al.* (2001). Therefore, both Re, and the Reynolds number of the cluster, defined as $Re_{cl} = U_{cl} R_{cl}/\nu$, are identically zero; here, U_{cl} is the mean settling velocity of the cluster, and R_{cl} a measure of its size. In comparison, the dilute clusters analysed in our study sediment with a mean velocity of the same order as that of a single particle ($U_{cl} \approx U$), the cluster dimension (R_{cl}) being much larger than aRe^{-1}. Thus, although $Re \ll 1$, we have $Re_{cl} \gg 1$. Nitsche & Batchelor (1997) examined the temporal evolution of an initially spherical inertialess suspension blob sedimenting in a quiescent fluid. The blob was found to retain its initial shape to a good approximation, while leaking particles from its rear in a vertical tail that eventually led to its breakup. Notwithstanding the small slip due to gravity of the particle phase, the flow around the suspension blob is, in fact, similar to that around a similar liquid drop with the same effective density, again in the absence of inertia (Batchelor 1974). The hydrodynamic interactions between particles in the blob, however, cause them to occasionally cross over into the particle-free liquid region, leading to their being swept around to the rear, and thence giving rise to the aforementioned tail.

This analogy between the behaviour of liquid drops and suspension blobs was formally proven by Machu *et al.* (2001) in the limit where the particles in the suspension blob are finely dispersed, and in addition, their distribution in the evolving blob remains statistically uniform; the latter was shown to be true in the simulations carried out. The sedimenting suspension drops remained spherical for an initial length of time, but eventually formed a torus that underwent breakup into two or more drops in a repeating cascade. This cascade is again similar to that known for a liquid drop settling in a second miscible liquid at low Reynolds numbers. The sequence of events leading to eventual breakup was found to be relatively insensitive to the initial shape of the suspension blob. More recent investigations report similar results (see Ekiel-Jezewska, Metzger & Guazzelli 2006; Metzger, Nicolas & Guazzelli 2007). In the above investigations, particles were treated as point forces (Stokeslets) and only the $O(1/r)$ far-field hydrodynamic interactions were included in an attempt to approximate dilute clusters.

The constraint of a dilute cluster is also necessary in the presence of inertia, since a rigorous treatment of multi-particle hydrodynamic interactions at small but finite Re is extremely difficult owing both to the nonlinearity and unsteady nature of the governing equations. The former does not allow superposition of independent solutions, for instance, and the latter implies a history dependence. Thus, even with the known velocity field around a single translating particle in the limit of weak inertia, the interaction between any pair of particles at finite Re at any instant of time is far more involved, being, in principle, dependent on the entire time history leading up to the current system configuration (see Koch 1993; Koch & Hill 2001). The effects of hydrodynamic interactions in the context of homogeneous sedimenting suspensions of spherical particles have been recently examined by Yin & Koch (2007). In the dilute limit, however, well-separated particles interact with each other only via weak disturbance velocity fields; it may be shown then that the time scale for a change in the particle configuration on account of interactions is much greater than the time taken for the vorticity to diffuse a distance comparable to the screening

length, and a quasi-steady scenario prevails even at non-zero Re. Similar reasoning suggests that inertia of the particles is also unimportant. Thus, each particle in a sufficiently dilute cluster is, in essence, passively convected by the disturbance velocity fields due to all other particles, and the characterization of cluster evolution reduces to drawing inferences about the kinematics of a group of tracer particles, each of which moves with the sum of its terminal settling velocity and the fluid velocity disturbances produced by the other particles.

The representation of a dilute cluster of any radius by a swarm of Stokeslets for sufficiently small Re, as has been the case in earlier studies, is incorrect. Such a representation is valid only when the inertial screening length is much smaller than the cluster size, because, for any finite Re, the fore–aft-symmetric Stokes approximation for the single-particle velocity disturbance is not a uniformly valid one in an unbounded fluid domain. It breaks down at length scales of $O(aRe^{-1})$ or greater when convection of the momentum defect can no longer be neglected. As indicated above, the velocity field at larger distances has an asymmetric source–wake structure. Since the nature of the velocity field differs radically in regions within and outside a distance of $O(aRe^{-1})$, even the evolution of a dilute cluster must be a strong function of its size relative to aRe^{-1}.

In order to determine the critical cluster size at which inertia becomes important, we first consider the opposite limit, that is, $Re_{cl} \ll 1$. Hydrodynamic interactions in the entire cluster are now dominated by viscous forces, and the cluster settles with a velocity $U_{cl} \sim R_{cl}^2 \phi(\rho_p - \rho_f)g/\mu$, where ϕ is the volume fraction of particles within the cluster. With $R_{cl} \gg a\phi^{-1/2}$, the slip velocities of the individual particles are negligible when compared with the cluster velocity, and one anticipates a continuum description to be valid. Recall that the cluster Reynolds number is defined as $Re_{cl} = U_{cl}R_{cl}/\nu$, and one therefore obtains $Re_{cl} \sim (R_{cl}/a)^3 \phi Re$. The condition $Re_{cl} \ll 1$ is evidently satisfied for any finite-sized cluster when $Re = 0$. The cluster behaves as a drop (see Nitsche & Batchelor 1997) with the constituent particles circulating in a familiar toroidal pattern. Thus, the fluctuation velocity of any particle (relative to its slip velocity U) will be $O(U_{cl})$. Note that a pair of sedimenting spheres maintain a constant relative separation at $Re = 0$ (see Happel & Brenner 1965), a fact related to the reversibility of the governing Stokes equations. Thus, the aforementioned drop-like dynamics and the resulting fluctuating velocities are a consequence of multi-particle interactions.

For Re small but finite, the spheres a pair move relative to each other even for separations smaller than $O(aRe^{-1})$. The Stokes equations being a valid leading-order approximation in this region, this relative velocity is only $O(Re)$. The relative velocity of a pair of particles separated by a distance r may be estimated from the far-field behaviour of the $O(Re)$ correction $\boldsymbol{u}_1$ to the Stokes velocity field ($\boldsymbol{u}_s$). Since $a \ll r \ll aRe^{-1}$, $\boldsymbol{u}_1$ is obtained from a regular perturbation expansion, and satisfies $\mu\nabla^2\boldsymbol{u}_1 - \nabla p_1 \approx \rho\, \boldsymbol{U} \cdot \nabla \boldsymbol{u}_s$ for $r \gg a$; since $\boldsymbol{u}_s \sim U(a/r)$ for $r \gg a$, one obtains $\boldsymbol{u}_1 \sim (\rho U/\mu) r^2 (Ua/r^2)$. Thus, the relative velocity of a particle pair, separated by a distance smaller than aRe^{-1}, is $O(ReU)$, and is such that a pair of particles in a transverse plane repel each other (Bretherton 1964). The velocity of a particle on account of all such inertial pair interactions is $\phi\,(R_{cl}/a)^3 ReU$. The fluctuation velocity on account of inertialess multi-particle interactions is still $O(U_{cl})$ for small Re. Equating the estimate for the fluctuation velocity due to inertial pair-interactions to the Stokes estimate, one obtains $R_{cl} \sim aRe^{-1}$ for the critical cluster size when 'micro-scale' inertia first becomes important. This is, in fact, a natural consequence of assuming inertial interactions to be pairwise additive in the dilute limit. Thus, the dominance of 'sub-screening length' inertial interactions will accompany a gradual

transition to pair-hydrodynamic interactions mediated by source–sink velocity fields. Both these interactions are described by the Oseen equations, and may be termed 'Oseen interactions', since these equations provide a uniformly valid approximation to $O(Re)$ in the region $r \gg a$. Oseen interactions are therefore expected to play a role in the evolution of sedimenting clusters with sizes comparable to or larger than the inertial screening length.

In the light of the above scaling arguments, an initially spherical cluster of size $a\phi^{-1/2} \ll R_{cl} \ll aRe^{-1}$ should behave as a drop, preserving its initial shape to a good approximation during sedimentation†, while a cluster larger than the critical size is expected to immediately deform, growing rapidly in its lateral dimensions on account of repulsive pair-particle interactions. Even in the suspension-drop regime, however, a cluster settles increasingly rapidly with an increase in size, as is evident from the expression for U_{cl} above. Eventually, the time taken for vorticity to diffuse across the cluster starts to become comparable to the time scale associated with the sedimentation of the cluster, and also the motion of particles within it. In other words, inertia on the scale of the cluster becomes important for large enough clusters. Comparison of the two time scales gives a critical cluster size of $O(aRe^{-1/3}\phi^{-1/3})$ for transition to a regime dominated by 'macro-scale' inertia. When $Re \ll \phi^{1/2}$, one has $a\phi^{-1/2} \ll aRe^{-1/3}\phi^{-1/3} \ll aRe^{-1}$, and the sedimenting cluster must first transition from the suspension-drop regime to a regime dominated by macro-scale inertia when $R_{cl} \sim aRe^{-1/3}\phi^{-1/3}$ (or $Re_{cl} \sim O(1)$); a second transition to a regime dominated by micro-scale inertia, discussed above, occurs when $R_{cl} \sim aRe^{-1}$. On the other hand, for $Re \gg \phi^{1/2}$, $a\phi^{-1/2} \gg aRe^{-1/3}\phi^{1/3} \gg aRe^{-1}$, and both the suspension drop and the intermediate macro-scale inertia regimes disappear.

For clusters with $R_{cl} < a\phi^{-1/2}$ for $Re < \phi^{1/2}$, and those with $R_{cl} < aRe^{-1}$ for $Re > \phi^{1/2}$, the slip velocity of a single particle is dominant, being larger than the induced velocity due to interaction with other particles in the cluster. These clusters do not exhibit the drop-like dynamics expected in the inertialess continuum limit, and may therefore be termed as sub-continnum clusters. Eventually, with increasing Re or R_{cl}, there is a transition to the regime studied in this paper wherein Oseen pair interactions determine cluster evolution. These transitions are summarized in figure 1. A naive extension of the Stokes drop analogy would have led one to conclude that sedimenting clusters at finite Re_{cl} should behave in a manner akin to miscible drops at the same Reynolds number. The scaling analysis emphasizes, however, that such a regime exists only in the limit $Re \ll \phi^{1/2}$. Finally, it is worth noting that with the onset of Oseen interactions, the velocity disturbance field driving the pair interaction decays with increasing distance. Correspondingly, pair interactions begin to weaken for separations greater than a screening length, the time scale for a change in the particle configuration increases, and clusters larger than $O(aRe^{-1})$ should continue to evolve in a quasi-steady fashion.

In general, a sedimenting cluster is expected to become increasingly dilute both via a continuous shedding of particles from its rear, and on account of an increase in size due to repulsive inertial pair-particle interactions. The former has been observed even in simulations carried out in the viscous-dominated regime namely. $Re = Re_{cl} = 0$ (see, Nitsche & Batchelor (1997)). As an example of the latter, even a cluster in the suspension drop regime must deform at any finite Re; of course, for $R_{cl} \ll aRe^{-1}$,

† The inevitable breakup of a Stokes sedimenting cluster, and subsequent formation of a torus, happens only after the cluster has settled through a rather long distance of the order of 30 times its own size (see Machu *et al.* 2001).

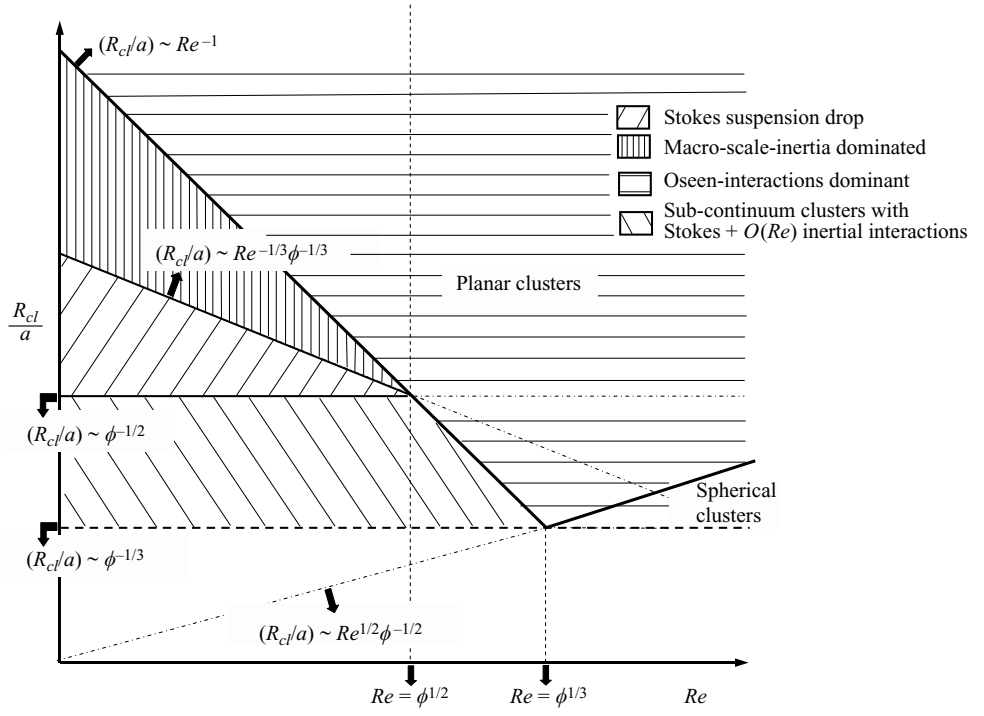

FIGURE 1. The various regimes of evolution for a sedimenting cluster of particles as a function of its size (R_{cl}), Re and ϕ (logarithmic scales). In the region corresponding to clusters dominated by Oseen interactions, the line $R_{cl}/a \sim Re^{1/2}\phi^{-1/2}$ denotes the critical value of the initial cluster radius separating distinct long-time evolution scenarios (see § 2).

the time scale for this deformation will be much longer than that required for the cluster to sediment through a distance of the order of its own size. Therefore, the Reynolds number Re_{cl} for any sedimenting cluster is expected to eventually become large enough for interparticle interactions to be governed by the Oseen equations.

In this paper, we therefore study what is likely to be the asymptotic long-time scenario for most sedimenting clusters: the quasi-steady evolution of a dilute ensemble of sedimenting particles in the limit $Re_{cl} \gg 1$, wherein the motion of each particle is governed by the Oseen-velocity fields due to all other particles in the cluster. The evolution of such clusters may differ significantly depending on whether interparticle interactions are dominated by the source ($O(1/r^2)$) or the wake ($O(1/r)$) part of the inertial velocity field. In the next section, we therefore present physical arguments which help differentiate between clusters whose evolution is dominated by wake interactions, and those that are driven by source–field interactions. The arguments suggest that the dynamics of a dilute sedimenting cluster with $Re_{cl} \gg 1$ will eventually be dominated by source–field interactions, but that the resulting expansion could either be two-dimensional (in a plane transverse to gravity) or three-dimensional depending on the radius of the initially spherical cluster. The critical cluster radius below which the expansion begins to transition from a three-to a two-dimensional one is found to be $O(N\nu/U)$. In either case, however, the dependence of the cluster size on N and t may easily be obtained by considering a particle at the edge of the expanding cluster; the (outward)bvelocity arising from repulsive pair interactions in

D dimensions is

$$\mathrm{d}R_{cl}/\mathrm{d}t \approx \int_0^{R_{cl}} O(1/r^2) n(r,t) r^{D-1} \mathrm{d}r,$$

where $D = 2$ or 3, and $n(r, t)$ is the appropriate number density in the evolving cluster. Since the total number of particles $N \sim \int n(r,t) r^{D-1} \mathrm{d}r$ remains constant, one may write instead, $\mathrm{d}R_{cl}/\mathrm{d}t \sim N/R_{cl}^2$, so the mean-square cluster size scales as $R_{cl}^2 \sim N^{2/3} t^{2/3}$, independent of D; in turn, this implies that the areal number density field in two dimensions must be $O(N/R_{cl}^2) \equiv O(N^{1/3}/t^{2/3})$, while the number density field in three dimensions must be $O(N/R_{cl}^3) \equiv O(1/t)$. It is worth noting that the cluster interactions in both cases are non-local, since the strength of interaction decays as $O(1/r^2)$, while the number of such interactions grows as $O(r^D)$ with $D \geqslant 2$. For small Re, the coefficient characterizing the strength of the source–field interactions may be obtained from Oseen's solution for the velocity field (see § 2). An analytical solution of the evolution equation for the number density field, and thence the numerical pre-factor in the expression for R_{cl} above, is readily obtained in three dimensions; in two dimensions, the aforementioned non-locality renders the determination of the numerical pre-factor particularly difficult. Nevertheless, the analysis predicts an axisymmetric planar cluster, as well as a spherical cluster with radial symmetry, to expand in a self-similar fashion, with the appropriate number density profiles being functions of the similarity variable $r/t^{1/3}$.

We now place our analysis in the context of previous related work on micro-scale inertia, both theoretical and experimental. To begin with, we mention the work of Vasseur & Cox (1977) who, via singular perturbation techniques, examined the interaction of a pair of sedimenting particles both in an unbounded fluid and in the presence of a plane boundary at small but finite Re. The separation between the particles was assumed to be much larger than the inertial screening length. For an unbounded fluid, their expression for the rate of separation of the spheres is identical to that resulting from our simplistic source–sink approximation for the far-field velocity disturbance field due to a single particle.

The earliest experiments on groups of settling particles are those of Jayaweera, Mason & Slack (1964). Among other things, the authors examined the motion of initially compact clusters of three or more spheres with Re ranging from 10^{-4} to about 5. For $Re < 1.5$, clusters of three to six spheres were found to eventually arrange themselves into regular polygons, oriented transversely to the direction of gravity, that continue to expand at a decreasing rate as they sediment; clusters of seven or more spheres exhibited no such regularizing tendency, however. A theoretical analysis by Hocking (1964), based on the Stokes equations, showed a regular polygonal arrangement of n spheres to be unstable for $n > 7$ in the limit where the interparticle separation is much larger than the radius of a sphere. Other results were left unexplained – for instance, the observed expansion of a sedimenting regular polygonal array is clearly beyond the scope of the reversible Stokes equations.

Later, Bretherton (1964) extended Hocking's analysis to include the first effects of inertia. In the limit $Re_{cl} \ll 1$, he showed that an expanding cluster of 3–6 spheres is an asymptotically stable configuration for long times, and oscillations about this state decay in amplitude owing to weakening interparticle interactions. Similar to the inertialess case, clusters of seven or more spheres were found to be unstable. For clusters with $Re_{cl} \gg 1$, Bretherton concluded, based on the interactions between the $O(1/r^2)$ radial source fields of the individual particles described above, that any polygonal arrangement would be weakly unstable. Although the Reynolds

numbers covered in Jayaweera *et al.*'s experiments were larger, and the separations between spheres smaller, than those strictly within the purview of Bretherton's theory, qualitative agreement between the two was still obtained, since the essential physics governing the cluster expansion remains unaltered at $O(1)$ values of the Reynolds number. For similar reasons, also discussed above, we expect the analysis in this paper to continue to describe dilute clusters even for $O(1)$ values of Re. It must be noted that the relative arrangement of spheres in the expanding polygonal arrays studied by Bretherton was fixed – the particles were located at the vertices of the polygon – and his analysis was in terms of the equations of motion for the individual particles. In contrast, we use a continuum field model here: the particle number density field in the evolving clusters is an unknown, and must be solved for together with the rate of expansion.

Recently, Leshansky, Lavrenteva & Nir (2003) analysed the settling of a finite assemblage of particles for times much longer than that taken for vorticity to diffuse across the cluster. The cluster was assumed to be compact, being much smaller than $aRe^{-1/2}$. As exported, the first effect of inertia was $O(Re)$. However, aside from the usual contributions arising from the local unsteady and convective acceleration terms in a region around the cluster of the order of its own size, and the convection of momentum in the Oseen region at distances of $O(aRe^{-1})$, the authors also found an additional singular contribution related to the unsteadiness of the cluster stresslet (owing to changes in its configuration) and originating at length scales of $O(aRe^{-1/2})$.

Finally, we mention the work of Kojima, Hinch & Acrivos (1984) who included inertial effects in their analysis of the experimentally observed expansion of a slender torus-shaped drop sedimenting in a second miscible liquid. Their analysis was again valid when the expanding torus is much smaller than $O(\nu/U)$. The nature of the $O(Re)$ inertial correction to the fore–aft-symmetric Stokes velocity disturbance (in this case, of each differential torus element) remains the same even at distances smaller than the screening length, being directed radially outward in a plane transverse to gravity, and thereby accounting for the observed expansion. The resulting rate of expansion is related to the spatial dependence of the inertial velocity correction, and therefore differs from that predicted for the clusters in our study; the $O(t^{2/3})$ growth is, of course, related to the $O(1/r^2)$ behaviour of the velocity disturbance at distances greater than the screening length. In summary, with the exception of Bretherton's study of polygonal particle arrays (see Bretherton 1964), other studies of sedimenting clusters have been restricted to the regime $R_{cl} \ll aRe^{-1/2}$, wherein the Stokes equations constitute a valid leading-order approximation for cluster evolution.

The paper is organized as follows. In § 2, we first present a qualitative description of cluster evolution in the limit $Re_{cl} \gg 1$; this is the expected long-time scenario based on earlier arguments. The description is based on the known far-field behaviour of the single-particle disturbance velocity field, for small but finite Re, and at distances greater than the inertial screening length. It is argued herein that the evolution of initially spherical clusters, for long times, is always driven by source–field interactions; however, there exists an initial period for smaller clusters when wake interactions play a crucial role in reducing the dimensionality of the long-time expansion that follows. We then derive the equation for the number density field in a sedimenting cluster whose evolution is driven by source–field interactions. The resulting nonlinear integro-differential equation lends itself to a similarity solution in both two and three dimensions. In either case, it becomes possible to reduce the original problem to the solution of a linear integral equation in similarity variables; this is done in § 3 for a spherical cluster. The integral equation in this case is readily solved, the number

density field within the cluster being a constant. In § 4.1, we describe the solution in two dimensions, in which case the self-similar number density field is spatially inhomogeneous; we merely write down the exact solution, leaving its rather involved derivation to Appendix A. For this case, we also derive the form of the number density field close to the centre of the cluster (§ 4.2); the number density field near the edge of the cluster is examined in Appendix B. The asymptotics serve as a useful aid in illustrating the physics governing the self-similar expansion in a planar cluster. The solutions for the number density field in both three and two dimensions are used to arrive at expressions for the corresponding cluster radii as functions of time. Finally, in § 5, we solve the full initial value problem for a planar cluster with a Gaussian profile for the initial areal number density field. The numerical integration is accomplished using the method of characteristics. The resulting number density profiles are found to collapse well for long times when re-plotted in similarity variables, confirming the asymptotic stability of the two-dimensional similarity solution, found in § 4, with respect to axisymmetric initial conditions. Section 6 presents a brief summary of the results along with some directions for future work.

2. Evolution of clusters driven by Oseen interactions

In this section, we present first a qualitative and thereafter a quantitative analysis of the evolution of clusters driven by far-field Oseen interactions. To start, we motivate the treatment of finite-Re pair-hydrodynamic interactions between sedimenting spherical particles

The Stokes equations fail to provide a uniformly valid approximation for the motion of a fluid around a sedimenting sphere. For small Re, the leading-order Stokes velocity field decays only algebraically, being $O(1/r)$ at large distances ($r \gg a$) from the sphere. The inertial terms then become important on length scales equal to or larger than $O(aRe^{-1})$ (the inertial screening length). With both convection and viscous diffusion comparably important, the inertial acceleration of a fluid element has to be included at leading order. In the limit $Re \ll 1$, a consistent leading-order approximation for the flow field in an unbounded domain is therefore given by the solution of the Oseen equations:

$$\rho \boldsymbol{U} \cdot \nabla \boldsymbol{u} = -\nabla p + \mu \nabla^2 \boldsymbol{u}, \tag{2.1}$$

$$\nabla \cdot \boldsymbol{u} = 0, \tag{2.2}$$

where $\rho \boldsymbol{U} \cdot \nabla \boldsymbol{u}$ represents convection of the velocity disturbance by the ambient uniform flow (in a reference frame moving with the sphere sedimenting with velocity $\boldsymbol{U}$). A solution, consistent with the degree of approximation in the equations themselves, is given by (see Batchelor 1967):

$$u_r = \frac{Ua^2}{r^2}\left[-\frac{a}{2r}\cos\theta - \frac{3(1-\cos\theta)r}{4a}\exp\left\{-\frac{Re\, r(1+\cos\theta)}{2a}\right\} + \frac{3}{2Re}\left(1-\exp\left\{-\frac{Re\, r(1+\cos\theta)}{2a}\right\}\right)\right], \tag{2.3}$$

$$u_\theta = Ua^2\left[\frac{a\sin\theta}{4r^3} - \frac{3\sin\theta}{4ar}\exp\left\{-\frac{Re\, r}{2a}(1+\cos\theta)\right\}\right], \tag{2.4}$$

in a spherical coordinate system with its polar axis coincident with the direction of translation. While still being linear, the Oseen equations are no longer reversible: a reversal in boundary motion ($\boldsymbol{U} \leftrightarrow -\boldsymbol{U}$) does not reverse time ($\boldsymbol{u}, p \leftrightarrow -\boldsymbol{u}, -p$).

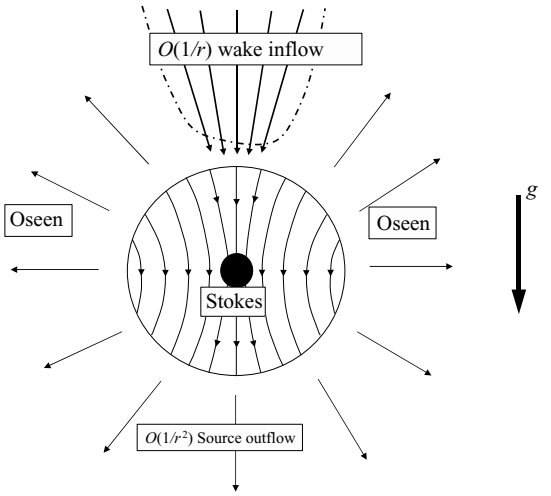

FIGURE 2. The source–sink character of the velocity field at distances greater than the inertial screening length ν/U.

Therefore, they do not give rise to a fore–aft-symmetric flow pattern. Although the near-field streamlines are approximately symmetric, indicating the validity of the Stokes approximation when $r \ll \nu/U$, the velocity field for $r \gg \nu/U$ looks dramatically different (see figure 2). The flow at these length scales becomes radial, as from a source of fluid at the sphere:

$$u_r \approx \frac{Q}{4\pi r^2}, \tag{2.5}$$

with $Q = 6\pi\nu a$, except within a narrow wake directly behind the sphere where the compensating inflow continues to decay as

$$u_r \approx -\frac{QU}{6\pi\nu r}, \tag{2.6}$$

similar to the inertialess limit; the radial extent of the wake grows as $r_{wake} \approx (\nu z/U)^{1/2}$ with downstream distance z.

In order to obtain a representation of the inertial interactions in the limit $Re \ll 1$, to be used in the ensuing arguments and analysis, we first note that the magnitude of the disturbance fields, at distances of $O(\nu/U)$ or greater, is at least $O(Re)$ smaller than the individual sedimenting velocities. A measure of the time required to set up the steady Oseen field, given by (2.3) and (2.4), is the time taken for the vorticity to diffuse across an inertial screening length, and is therefore $O(\nu/U^2)$. It may then easily be shown that the time scale, $R/\dot{R}$, for an increase in the separation R of a particle–pair, interacting via (weak) source fields, is much greater than $O(\nu/U^2)$ so long as $R \gg aRe^{-2/3}$; the latter is, of course, true, since, for small Re, the scenario discussed above only starts to hold when $R > aRe^{-1} \gg aRe^{-2/3}$. This implies that the unsteadiness of the fluid velocity field on account of the evolving pair geometry may be neglected. From the particles' equation of motion, the time scale of acceleration associated with the source velocity field scales as $(mRe/\mu U)^{1/2}(R/a)^{3/2}$, $m = \frac{4}{3}\pi\rho_p a^3$ being the mass of the particle; the inertial relaxation time of the particle, $\tau_p = (m/6\pi\eta a)$, remains small in comparison provided $(\rho_p/\rho_f)^{1/2}(a/R)^{3/2} \ll 1$. Since $R \gg aRe^{-1}$, a sufficient condition for particle inertia to be negligible is $\rho_p/\rho_f \ll Re^{-3}$ for $Re \ll 1$. In a frame of reference

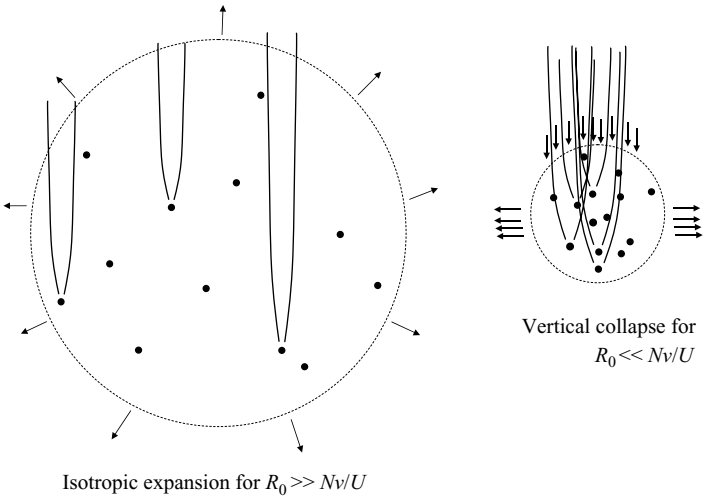

FIGURE 3. The differing evolution of a cluster, driven by Oseen interaction, as a function of its initial size R_0.

moving with velocity U, each particle then moves with a velocity that is the sum of the velocity fields due to all the other particles in the cluster, each given by (2.3) and (2.4) in the limit $r \gg \nu/U$, evaluated at its centre.

Based on the expressions (2.5) and (2.6) for the far-field velocity disturbance in the source and wake regions of a sedimenting particle, we now discuss the evolution of an initially spherical cluster on account of Oseen interactions. The nature of the evolution is a function of the initial cluster size (R_0, say), and the number of particles (N). Since the volume of a single-particle wake within the cluster is $O(\nu R_0^2/U)$, the probability that a particle will find itself in the wake of any other particle is given by the ratio of the volume of N such wakes to the initial volume of the cluster; this is $O(N\nu R_0^2/UR_0^3) \equiv O(N\nu/R_0U)$. Clearly, if $R_0 \gg N\nu/U$, most particles in the initial cluster are outside the wake of any other particle, and the evolution of the cluster is governed primarily by repulsive source–field interactions (see figure 3). Thus, an initially spherical cluster with $R_0 \gg O(N\nu/U)$ remains spherical, and its radius increases with time. The probability of wake interactions, if small at the initial instant, will become even smaller with increasing cluster size.

On the other hand, when $R_0 \ll O(N\nu/U)$, each particle is initially in the wake of many other particles; there are, in fact, $O(N\nu/R_{cl}U)$ such particles, R_{cl} being the cluster radius at time t. Since $R_{cl} \gg \nu/U$, this number is still much smaller than N. Thus, each particle continues to experience an outward source flow due to $O(N)$ other particles, that is $O(QN/R_{cl}^2)$, and that, when acting in isolation, would drive an isotropic expansion of the cluster. There is, however, an additional inward flow in the vertical direction due to the particle wakes. Each wake gives rise to a flow of $O(QU/\nu R_{cl})$, so the inward flow produced by $O(N\nu/R_{cl}U)$ wakes is again $O(QN/R_{cl}^2)$; this is comparable to, and tends to offset, the source-flow-driven expansion in the vertical direction. In fact, since this flow is always dominant in the transverse directions, the resulting outflow in a transverse plane has to be balanced by a net inward flow in the vertical direction. One therefore expects the wake contribution to be greater, with the result that the aspect ratio of a cluster with $R_0 \ll O(N\nu/U)$ should decrease (see figure 3).

Now if Z_{cl} denotes the (smaller) vertical dimension of a cluster at time t, then the cluster volume is $O(Z_{cl}R_{cl}^2)$, while the wake of a single particle occupies a volume of $O(\nu Z_{cl}^2/U)$ inside the cluster; this implies that each particle finds itself in the wake of $O(NZ_{cl}\nu/UR_{cl}^2)$ other particles. Since the vertical velocity in each wake is $O(Q\nu/UZ_{cl})$, the net inward flow due to wakes is again $O(QN/R_{cl}^2)$. On the other hand, the smaller aspect ratio, Z_{cl}/R_{cl}, of the cluster implies that the vertical component of the radial source flow is weaker by $O(Z_{cl}/R_{cl})$, being only $O(QNZ_{cl}/R_{cl}^3)$. Thus, once the cluster starts to flatten, the source flow becomes of a smaller order than the wake flow in the vertical direction, and the vertical collapse of the cluster will continue. This collapse should persist until one reaches a point where a typical particle is no longer in the wake of any other particle. This occurs when $Z_{cl}/R_{cl} \approx O(R_{cl}U/N\nu)$. Since the wake and source-flow contributions were of the same order to begin with, the collapse in the z-direction should occur in a time over which the transverse dimension of the cluster is still of the same order as its initial value R_0. This implies that the aspect ratio attained by the cluster at the end of this collapse is $O(R_0U/N\nu)$. This aspect ratio is asymptotically small in the regime where there are many wake interactions per particle in the initial cluster. In this flattened cluster, a typical particle no longer has a wake interaction, and the evolution for all later times is therefore driven by source flows alone. From scaling arguments used in the introduction, now modified for a non-spherical cluster, $\mathrm{d}R_{cl}/\mathrm{d}t \approx NQ/R_{cl}^2$ and $\mathrm{d}Z_{cl}/\mathrm{d}t \approx NQZ_{cl}/R_{cl}^3$ for the source–field-driven expansion. These equations are consistent with an evolution at a constant aspect ratio, so the aspect ratio remains $O(R_0U/N\nu)$ for later times.

To summarize then, provided $R_0 \gg N\nu/U$, one obtains an expanding spherical cluster for all times, the expansion being due to radial source–field interactions. A cluster of asymptotically small aspect ratio results if $R_0 \ll N\nu/U$; the resulting flattened configuration begins to expand thereafter, again on account of source–field interactions, but now occurring predominantly in a plane transverse to gravity. Finally, an intermediate scenario is expected if $R_0 \sim O(N\nu/U)$; an initially spherical cluster should, in this case, evolve into a cluster with an aspect ratio of the same order as, but less than, unity, and subsequent evolution will again be driven by source–field interactions. The above limits may be rewritten in terms of the cluster volume fraction, $\phi \sim Na^3$, and one then obtains $R_0 \sim O(aRe^{1/2}\phi^{-1/2})$ for the critical size of the initial cluster; this is illustrated in figure 1. It must be noted that the location of spherical and planar clusters (as the relevant long-time limits) relative to the critical cluster size is reversed when considering clusters at constant ϕ. Thus, it is clusters smaller than $O(Re^{1/2}\phi^{-1/2})$ which evolve into nearly planar configurations; this is, of course, because increasing cluster size with a constant ϕ corresponding to an increase in N proportional to the cube of the cluster radius.

In the next two sections, we analyse quantitatively the long-time evolution of a cluster, in both two and three dimensions, driven by source–field interactions. Using (2.5), we observe that the velocity at any point $\boldsymbol{r} \equiv (x, y)$ in the cluster, in a reference frame moving with its settling velocity, may now be written as

$$\boldsymbol{u}(\boldsymbol{r}, t) = \frac{Q}{4\pi} \int \frac{(\boldsymbol{r} - \boldsymbol{r}')}{|\boldsymbol{r} - \boldsymbol{r}'|^3}\, n(\boldsymbol{r}', t)\, \mathrm{d}\boldsymbol{r}', \tag{2.7}$$

where $n(\boldsymbol{r}, t)$ is the number density field, denoting the number of particles per unit area in two dimensions, and those per unit volume in three dimensions. Conservation of the total number (N) of particles, when expressed in differential form, leads to a

continuity equation for the number density field:

$$\frac{\partial}{\partial t} n(\boldsymbol{r}, t) + \nabla \cdot (\boldsymbol{u}(\boldsymbol{r}, t) n(\boldsymbol{r}, t)) = 0. \tag{2.8}$$

In (2.7) and (2.8), we have adopted a continuum description of the discrete-particle cluster in terms of number density and induced velocity fields: $(n(\boldsymbol{r}, t), \boldsymbol{u}(\boldsymbol{r}, t))$. The convolution integral in (2.7) results because the velocity of any differential cluster element results from a superposition of the source velocity fields due to the remaining part of the cluster.

We restrict consideration to cases where the number density field is independent of angular coordinates. Symmetry arguments immediately imply that the induced velocity at any point in such a cluster, in both two and three dimensions, only has a radial component, and that the number density in either case is a function of the radial coordinate alone. Equations (2.7) and (2.8) take the form

$$u_r(r, t) = \frac{Q}{2\pi} \int_0^{\infty} \int_0^{2\pi} \frac{(r - r' \cos\phi) n(r', t)}{(r^2 + r'^2 - 2rr' \cos\phi)^{3/2}} \, \mathrm{d}\phi \, r'^2 \mathrm{d}r', \tag{2.9}$$

$$\frac{\partial n}{\partial t} + \frac{1}{r^2} \frac{\partial}{\partial r} [u_r(r, t) r^2 n] = 0, \tag{2.10}$$

for a spherical cluster, and

$$u_r(r, t) = \frac{Q}{4\pi} \int_0^{\infty} \int_0^{2\pi} \frac{(r - r' \cos\phi) n(r', t)}{(r^2 + r'^2 - 2rr' \cos\phi)^{3/2}} \, \mathrm{d}\phi \, r' \mathrm{d}r', \tag{2.11}$$

$$\frac{\partial n}{\partial t} + \frac{1}{r} \frac{\partial}{\partial r} [u_r(r, t) r n] = 0, \tag{2.12}$$

for an axisymmetric planar cluster. Here, r is the radial distance from the centre of the cluster, and ϕ is the azimuthal angle in a plane defined by $\boldsymbol{r}$ and $\boldsymbol{r}'$, the integration having been carried out over a polar angle perpendicular to this plane; for a planar cluster, this plane is oriented perpendicular to gravity.

3. Self-similar evolution of spherical clusters

For spherical clusters, the expression, (2.9), for the induced velocity field may be simplified by observing that the source outflow associated with a single spherical particle satisfies $\nabla \cdot \boldsymbol{u} = Q\delta(\boldsymbol{x})$; the conservation of mass is apparently violated because we neglect the compensating wake inflow. For a spherical cluster with number density $n(\boldsymbol{r}, t)$, one therefore has $\nabla \cdot \boldsymbol{u} = Qn$. Integrating over a spherical volume, and using radial symmetry, we then obtain

$$u_r(r, t) = \frac{Q}{r^2} \int_0^{r'} n \, r'^2 \mathrm{d}r'. \tag{3.1}$$

It is readily shown that evaluation of the angular integral in (2.9) leads to the same result. Using (3.1) in (2.10), we have

$$\frac{\partial n}{\partial t} + \frac{Q}{r^2} \frac{\partial}{\partial r} \left[\left(\int_0^r n r'^2 \mathrm{d}r' \right) n \right] = 0. \tag{3.2}$$

The absence of a characteristic length scale for the number density profile is evident in the continuum description given by (3.2). We therefore anticipate a similarity solution, with the number density depending only on a particular combination of space and

time variables. Equation (3.2) may, in fact, be regarded as a nonlinear dispersion equation with a 'dispersion' coefficient proportional to Q, i.e. with dimensions of $(length)^3/time$; this immediately suggests, as will also be shown rigorously below, a similarity variable proportional to $r/t^{1/3}$.

We now employ the standard similarity formulation, namely $n(r,t) = f(t)\hat{g}(\bar{\eta})$, with the similarity variable $\bar{\eta} = r/t^{\gamma}$, where both the function $f(t)$ and exponent γ will be determined from the requirements that the total number of particles conserved, and that the equation for $\hat{g}$ which results on transforming (3.2), be entirely in terms of $\bar{\eta}$. On transforming, we obtain

$$\frac{\mathrm{d}f}{\mathrm{d}t}\,\hat{g} - \gamma\,\bar{\eta}\frac{f(t)}{t}\frac{\partial \hat{g}}{\partial \bar{\eta}} = -\frac{f^2(t)}{t^{\gamma}}\frac{Q}{\bar{\eta}^2}\frac{\partial}{\partial \bar{\eta}}\left[\hat{g}(\bar{\eta})\int_0^{\bar{\eta}}\hat{g}(\bar{\eta}')\bar{\eta}'^2 d\bar{\eta}'\right]. \tag{3.3}$$

For a similarity solution to work, there must be no explicit time dependence in the transformed equation, which implies an equality of t-dependence of all terms in (3.3); thus,

$$\frac{\mathrm{d}f}{\mathrm{d}t} \equiv \frac{f(t)}{t} \equiv f^2(t).$$

This requires $f(t) \sim (1/t)$ with γ still arbitrary. Thus, a similarity solution must be of the form $n = (1/t)\hat{g}(r/t^{\gamma})$. The additional integral constraint of a constant number of particles, $N \sim \int nr^2\mathrm{d}r$, gives $\gamma = 1/3$, as expected. This immediately implies that the mean-square size of the planar cluster grows as $t^{2/3}$, since

$$\begin{aligned}\langle r^2\rangle &= 4\pi\int r^2 n(r,t) r^2\,dr,\\ &= 4\pi t^{(5\gamma-1)}\int \bar{\eta}^4\hat{g}(\bar{\eta})d\bar{\eta},\\ &= Kt^{2/3}\end{aligned}$$

where the proportionality constant $K = 2\pi\int\bar{\eta}^4\hat{g}(\bar{\eta})\mathrm{d}\bar{\eta}$ depends on the exact functional form of $\hat{g}$; the latter, of course, entails solving equation (3.3).

We now define the non-dimensional similarity variable, $\eta = \bar{\eta}/Q^{1/3} = r/(Qt)^{1/3}$, and, in addition, use $\hat{g} = g/Q$, where $g(\eta)$ is now the dimensionless number density in similarity variables (the original number density field is therefore given by $n = g/(Qt)$). This then serves to absorb the pre-factor Q in (3.3), leading to the following equation for $g(\eta)$:

$$-g - \frac{1}{3}\eta\frac{\mathrm{d}g}{\mathrm{d}\eta} = -\frac{1}{\eta^2}\frac{\mathrm{d}}{\mathrm{d}\eta}\left[g\int_0^{\eta} g(\eta')\eta'^2\mathrm{d}\eta'\right]. \tag{3.4}$$

Re-writing (3.4) as

$$\frac{\mathrm{d}}{\mathrm{d}\eta}(g\eta^3) = 3\frac{\mathrm{d}}{\mathrm{d}\eta}\left[g\int_0^{\eta} g(\eta')\eta'^2\mathrm{d}\eta'\right], \tag{3.5}$$

we observe that it has a first integral given by

$$g\eta^3 = 3g\int_0^{\eta} g(\eta')\eta'^2\mathrm{d}\eta' + \mathscr{C}_1. \tag{3.6}$$

Here, $\mathscr{C}_1$ is an integration constant that may be determined from the limiting form of (3.6) for $\eta \to \infty$. One expects the evolving spherical cluster to have a finite variance at all times. Stated in similarity variables, $\int_0^{\infty} g\eta^4\mathrm{d}\eta$ must be finite, implying that $g \sim o(\eta^{-5})$ for $\eta \gg 1$; the term $g\eta^3$ in (3.6) is thus asymptotically small for

large η. As seen from (3.1) and (3.2), the second term in (3.6) is proportional to the radial velocity, expressed in similarity variables, induced by a sedimenting spherical cluster. For a compact cluster, this velocity may be approximated as $(Q/2\pi)\int_0^\infty n(r',t)r'^2\,\mathrm{d}r'/r^2 \approx O(QN/r^2)$ when $r \gg R_{cl}(t)$, R_{cl} being a measure of the cluster dimension at time t. It is therefore of $O(\eta^{-2})$ at large distances, implying that for large η, the second term in (3.6) is $O(g/\eta^2)$, again being vanishingly small. Taking the limit $\eta \to \infty$ in (3.6), we then obtain $\mathscr{C}_1 = 0$; alternatively, the condition may also be seen as the requirement for a finite g at $\eta = 0$.

Setting $\mathscr{C}_1 = 0$, the following linear integral equation for $g(\eta)$ results:

$$3\int_0^\infty g(\eta')\eta'^2\mathrm{d}\eta' = \eta^3. \tag{3.7}$$

Physically, (3.7) represents a balance, at any fixed Cartesian point, between the outward radial velocity induced by the evolving cluster, and the virtual inward velocity that arises in transforming to (temporally) expanding similarity coordinates. This is, of course, a requisite for a steady solution in the transformed coordinate system. (A variant of this physical argument – that there must be no net flux at infinity – could also have been used to conclude that the constant of integration $\mathscr{C}_1$ in (3.6) must indeed equal zero.) As argued earlier, the left-hand side of (3.7), being proportional to the induced radial velocity, must, in the limit $\eta \gg 1$, decay as $O(\eta^{-2})$ for any compact cluster. Thus, any integrable number density profile, i.e. a $g(\eta)$ with $\int_0^\infty g(\eta)\eta^2\mathrm{d}\eta$ finite, will never support a cubic increase in the induced radial velocity over an infinite range. For the equality in (3.7) to hold, one must therefore have a finite cluster. Denoting the radial dimension of the cluster in similarity coordinates by η_m (this translates to a time-dependent cluster size ($\propto \eta_m t^{1/3}$) in the original variables), one only requires (3.7) to be satisfied in the interval $(0, \eta_m)$. This is evident from (3.6), where with $\mathscr{C}_1 = 0$, one observes that a trivial g, as would be the case outside a finite cluster, is also a solution.

We now wish to solve

$$3\int_0^{\eta_m} g\eta'^2\mathrm{d}\eta' = \eta^3 \quad (\eta \leqslant \eta_m). \tag{3.8}$$

That $g = 1$ solves (3.8) is immediate. Thus, the number density field in the self-similarly expanding spherical cluster is $n(r,t) = 1/(Qt)$. The dimensional radius of the cluster (R_{cl}) at time t is easily found, since $n(\frac{4}{3}\pi R_{cl}^3) = N$, whence we obtain

$$R_{cl}(t) = \left(\frac{3NQt}{4\pi}\right)^{1/3}, \tag{3.9}$$

$$= 1.651(N\nu a)^{2/3}t^{2/3}, \tag{3.10}$$

on using $Q = 6\pi\nu a$. Thus, the dilute spherical cluster, at small but finite Re, undergoes a slow self-similar expansion. The rate of expansion decreases with increasing time as $t^{-2/3}$, since the repulsive finite-Re interactions that drive the cluster expansion weaken with increasing interparticle separation. A second measure of the cluster size, the variance of the positions of all the cluster particles, may be calculated as

$$\langle r^2\rangle = \frac{\displaystyle\int_0^{R_{cl}(t)} [r^2 n(r,t)]r^2\mathrm{d}r}{\displaystyle\int_0^{R_{cl}(t)} n(r,t)r^2\mathrm{d}r}, \tag{3.11}$$

and is given by $\langle r^2\rangle = (3/5)R_{cl}^2$ for a constant number density field.

4. Self-similar evolution of planar clusters

4.1. *The number density profile in a self-similarly expanding planar cluster*

In § 2, it was argued that the initial dominance of wake interactions in spherical clusters with radii smaller than $O(N\nu/U)$ alters the dimensionality of the ensuing source–field-driven expansion. The cluster rapidly deforms into a flattened configuration, and subsequent expansion occurs in a plane transverse to gravity. The analysis in this section is restricted to this regime, and we consider the limiting scenario of an axisymmetric planar cluster. The predictions of the analysis are expected to be accurate for clusters with an aspect ratio much smaller than unity ($Z_{cl} \ll R_{cl}$), even they are not perfectly planar (that is, if $Z_{cl} > O(a)$). For this case, equations (2.11) and (2.12) apply; integration over the azimuthal coordinate in (2.11) gives

$$u_r(r,t) = -\frac{Q}{2\pi}\left[\int_0^r \frac{\mathrm{d}}{\mathrm{d}r}\left\{\frac{1}{r}K\left(\frac{r'}{r}\right)\right\} n(r',t)r'\mathrm{d}r' + \int_r^\infty \frac{\mathrm{d}}{\mathrm{d}r}\left\{K\left(\frac{r}{r'}\right)\right\} n(r',t)\mathrm{d}r'\right], \tag{4.1}$$

for the radial component of the induced velocity field, and the following nonlinear integro-differential equation for the areal number density field:

$$\frac{\partial n(r,t)}{\partial t} = \left(\frac{Q}{2\pi}\right)\frac{1}{r}\frac{\partial}{\partial r}\left[rn(r,t)\int_0^\infty \left\{\frac{\mathrm{d}}{\mathrm{d}r}\left(\frac{1}{r}K\left(\frac{r'}{r}\right)\right)r' + \left[\frac{\mathrm{d}}{\mathrm{d}r}\left(K\left(\frac{r}{r'}\right)\right) - \frac{\mathrm{d}}{\mathrm{d}r}\left(\frac{1}{r}K\left(\frac{r'}{r}\right)\right)r'\right]H(r'-r)\right\} n(r',t)\mathrm{d}r'\right]. \tag{4.2}$$

Here, $H(x)$ is the heavyside function, and $K(x)$ is the complete elliptic integral of the first kind, being defined as (see Gradshteyn & Ryzhik 1965)

$$K(x) = \int_0^{\pi/2} \frac{\mathrm{d}p}{\sqrt{1-x^2\sin^2 p}}.$$

Equation (4.2), governing the number density profile in a planar sedimenting cluster, is evidently more complicated than that in three dimensions (see equation (3.2)); the complexity appears to result from the fact that the $O(1/r^2)$ source–field interactions, intrinsic to three dimensions, now operate in a two-dimensional space. Nevertheless, a similarity transformation, identical to that used in § 3, also works in two dimensions, and we obtain $n(r,t) = 1/(Qt)^{2/3}g(r/t^{1/3})$ for the areal number density field in the evolving planar cluster. Again, defining a normalized similarity variable, $\eta = r[2\pi/(Qt)]^{1/3}$, we obtain the following equation for the function g:

$$-\frac{2}{3}g - \frac{1}{3}\eta\frac{\mathrm{d}g}{\mathrm{d}\eta} = \frac{1}{\eta}\frac{\mathrm{d}}{\mathrm{d}\eta}\left[g\eta\int_0^\infty G(\eta,\eta')g(\eta')\mathrm{d}\eta'\right], \tag{4.3}$$

where $G(\eta,\eta')$, the integral kernel in transformed variables, is given by

$$G(\eta,\eta') = \frac{\mathrm{d}}{\mathrm{d}\eta}\left(\frac{1}{\eta}K\left(\frac{\eta'}{\eta}\right)\right)\eta' + \left[\frac{\mathrm{d}}{\mathrm{d}\eta}\left(K\left(\frac{\eta}{\eta'}\right)\right) - \frac{\mathrm{d}}{\mathrm{d}\eta}\left(\frac{1}{\eta}K\left(\frac{\eta'}{\eta}\right)\right)\eta'\right]H(\eta'-\eta). \tag{4.4}$$

Arguments identical to those used in three dimensions finally lead to the following linear integral equation for g:

$$-3\int_0^\infty G(\eta,\eta')g(\eta')\mathrm{d}\eta' = \eta. \tag{4.5}$$

We again conclude that g can only be non-zero over a finite range. Denoting the upper limit of this range as η_m, it is required to solve

$$-3\int_0^{\eta_m} G(\eta,\eta')g(\eta')\mathrm{d}\eta' = \eta \qquad (\eta \leqslant \eta_m), \tag{4.6}$$

in order to obtain the number density field in the expanding cluster. In (4.6), the kernel $G(\eta,\eta')$ is of the 'split' type, being defined differently in the ranges $(0,\eta)$ and (η,η_m):

$$\begin{aligned} G(\eta,\eta') &= \frac{\mathrm{d}}{\mathrm{d}\eta}\left(\frac{1}{\eta}K\left(\frac{\eta'}{\eta}\right)\right)\eta' \quad \text{for} \quad 0 \leqslant \eta' < \eta, \\ &= \frac{\mathrm{d}}{\mathrm{d}\eta}\left(K\left(\frac{\eta}{\eta'}\right)\right) \quad \text{for} \quad \eta \leqslant \eta' < \eta_m. \end{aligned}$$

Using the properties of the elliptic function $K(x)$, in particular that its derivative, $K'(x)$, behaves as $1/(1-x)$ for $x \to 1$, the kernel $G(\eta,\eta')$ may be written in the form

$$G(\eta,\eta') = K_R(\eta,\eta') + K_S(\eta,\eta'), \tag{4.7}$$

where $K_R(\eta,\eta')$ only has a weak logarithmic singularity at $\eta = \eta'$, while $K_S(\eta,\eta')$, the singular part, is proportional to $1/(\eta-\eta')$ for $|\eta-\eta'| \ll 1$. Thus, (4.6) is, in fact, a singular integral equation of the first kind, and the integral therein must be interpreted as a Cauchy principal value. The properties of the solutions of such equations differ quite significantly from that known from the Fredholm theory for regular kernels (Muskhelishvili 1992; Gakhov 1966).

The aforementioned singularity of the kernel arises due to the assumed $O(1/r^2)$ interactions between sedimenting particles; thus, the strength of a pair interaction diverges at infinitesimal separations at a rate faster than the $O(1/r)$ divergence for Stokeslets. On one hand, this divergence is clearly aphysical since the theory is only valid for interparticle separations greater than the inertial screening length. In other words, the assumed form of the interactions (see equation (2.5)) is not uniformly valid in r, being inapplicable in the range $r < O(aRe^{-1})$. Therefore, the interpretation of the integral involving $K_S(\eta,\eta')$ as a Cauchy integral physically corresponds to eliminating the divergent short-range repulsive interactions at any point in the planar cluster. A better interpretation emerges on relating to an actual particulate cluster where the far-field $O(1/r^2)$ interactions, at distances larger than the inertial screening length, must transition to a non-singular interaction in the region near $r = 0$ (the sub-screening-length inertial interactions discussed earlier). Clearly, a non-zero induced velocity field at any given point in the cluster must arise only due to asymmetric non-singular interactions in the near-field and far-field isotropic interactions mediated via an angular asymmetry in the number density field around the point. Isotropic interactions due to a number density field that is radially symmetric about a given point will not contribute to an induced velocity at that point. In our analysis, the near-field interactions are not considered since the interparticle separation is assumed to be much larger than the screening length; in addition, isotropic interactions obey an inverse square law, and therefore turn out to be divergent for a planar cluster. The Cauchy principal value interpretation then serves to eliminate the contribution of isotropic interactions from the radially symmetric component of the areal number density field around any given point.

Writing the integral containing the split kernel in (4.6) as two separate integrals, we obtain:

$$\int_0^{\eta} \frac{\mathrm{d}}{\mathrm{d}\eta}\left(\frac{1}{\eta}K\left(\frac{\eta'}{\eta}\right)\right) g(\eta')\eta'\,\mathrm{d}\eta' + \int_{\eta}^{\eta_m} \frac{\mathrm{d}}{\mathrm{d}\eta}\left(K\left(\frac{\eta}{\eta'}\right)\right) g(\eta')\mathrm{d}\eta' = -\frac{\eta}{3} \quad (\eta \leqslant \eta_m). \tag{4.8}$$

It is shown in Appendix A that the solution to (4.8) is of the form

$$g = g(0)(1-\eta^2/\eta_m^2)^{1/2}, \tag{4.9}$$

with $g(0)$ being the value of g at the centre of the cluster. This number density profile yields an induced velocity linear in η for $\eta \leqslant \eta_m$. A relation between $g(0)$ and η_m may, in principle, be obtained by substituting (4.9), performing the resulting integrals in (4.8), and finally, equating coefficients of η on both sides. Rather remarkably, an exact expression for the induced velocity, in a far more amenable form, may be derived using a perturbation expansion valid near the centre of the cluster. The simplified equations that are found in this limit also yield valuable insight into the physics of the planar cluster expansion. In the following subsection, we therefore solve (4.8) in a perturbative manner in a region close to the centre of the expanding cluster ($\eta \to 0$). In Appendix B, we derive the asymptotic form of the number density field near the edge of the planar cluster, that is, $g(\eta)$ for $\eta \to \eta_m$.

4.2. *The number density profile near the centre of the planar cluster*

Here, we formulate a perturbation solution for small η. To this end, it is convenient to recast (4.8) so the η dependence of the integral on the left-hand side appears in a more tractable form. We employ the following changes of variables: $\eta' = s\eta$ in the first integral, and $\eta' = \eta/s$ in the second, whence (4.8) takes the form

$$\int_0^1 s[K(s)+sK'(s)]g(\eta s)\,\mathrm{d}s + \int_1^{\eta/\eta_m} \frac{1}{s}\,g\left(\frac{\eta}{s}\right) K'(s)\,\mathrm{d}s = \frac{\eta}{3}. \tag{4.10}$$

We assume a cluster profile of the form

$$g(\eta) = g(0) - c\,\eta^{\alpha} + o(\eta^{\alpha}), \tag{4.11}$$

close to the centre, where c is a constant and the exponent $\alpha\,(>0)$ will be determined from the analysis. While the above expression yields a leading-order estimate for the first term in (4.10), it is necessary to use the full expression for $g(\eta)$ in the second term. Indeed, substituting (4.11) into (4.10) yields a divergent integral. The first term on the left-hand side in (4.10) is well-behaved for small η, the logarithmic singularity of $K(s)$ for $s \to 1$ being an integrable one. The stronger singularity of $K'(s)$ for $s \to 1$ does yield a logarithmically divergent integral; however, this singularity is cancelled by an identical singularity of opposite sign in the second term which also involves $K'(s)$. This cancellation is consistent with interpreting the original integral involving $G(\eta, \eta')$ in (4.6) as a Cauchy principal value. Thus, the divergence arises from the second term in (4.10) near $s = 0$, and may easily be seen using the small-η expansion for g in this term:

$$\int_1^{\eta/\eta_m} \frac{1}{s}\,g\left(\frac{\eta}{s}\right) K'(s)\,\mathrm{d}s = g(0)\int_1^{\eta/\eta_m} \frac{K'(s)}{s}\,\mathrm{d}s + c\,\eta^{\alpha}\int_{\eta/\eta_m}^1 \frac{K'(s)}{s^{1+\alpha}}\,\mathrm{d}s. \tag{4.12}$$

Now, $K'(s) \approx (\pi/4)s$ for $s \ll 1$; thus, replacing the lower limit in the second integral in (4.12) by zero, this term is found to be divergent for $\alpha > 1$, which is indeed the case, and the analysis below gives $\alpha = 2$ (see (4.18)). In other words, even for $\eta \to 0$, the integral involving $g(\eta/s)$ depends on the detailed number density profile over the

entire extent of the cluster and may not be approximated by the asymptotic form (4.11). Physically, the logarithmic divergence for $s \to 0$ that results on substituting (4.11) signifies the non-local nature of the cluster interactions contributing to the induced velocity in the planar cluster, as observed earlier in the introduction.

Keeping in mind therefore that the induced velocity will, even for small η, depend on $g(\eta)$ for η in the entire range $(0, \eta_m)$, we rewrite the left-hand side of (4.10) as follows:

$$\begin{aligned}
&\lim_{\eta\ll1}\left[\int_0^1 s[K(s)+sK'(s)]g(\eta s)\,\mathrm{d}s+\int_1^{\eta/\eta_m}\frac{1}{s}\,g\left(\frac{\eta}{s}\right)K'(s)\,\mathrm{d}s\right]\\
&\quad=\lim_{\eta\ll1}\left\{g(0)\left[\int_0^1 s[K(s)+sK'(s)]\,\mathrm{d}s-\int_{\eta/\eta_m}^1\mathrm{d}s\frac{K'(s)}{s}\right]\right.\\
&\quad\left.-c\,\eta^\alpha\int_0^1 s^{1+\alpha}[K(s)+sK'(s)]\,\mathrm{d}s-\int_{\eta/\eta_m}^1\mathrm{d}s\left[g\left(\frac{\eta}{s}\right)-g(0)\right]\frac{K'(s)}{s}\right\}. \qquad (4.13)
\end{aligned}$$

The first term on the right-hand side of (4.13) corresponds to replacing the actual number density profile $g(\eta)$ by a top-hat profile of height $g(0)$ and extent η_m. For such a profile, a non-zero induced velocity results only because of its finite extent; this may be seen explicitly by rewriting the first term in (4.13) as

$$\begin{aligned}
&g(0)\left[\int_0^1 s[K(s)+sK'(s)]\,\mathrm{d}s-\lim_{\eta\ll1}\int_{\eta/\eta_m}^1\mathrm{d}s\,\frac{K'(s)}{s}\right],\\
&\quad=g(0)\left[\int_0^1 s\left\{[K(s)+sK'(s)]s-\frac{K'(s)}{s}\right\}\mathrm{d}s+\lim_{\eta\ll1}\int_0^{\eta/\eta_m}\mathrm{d}s\,\frac{K'(s)}{s}\right] \qquad (4.14)\\
&\quad=\left(\frac{\pi}{4}\frac{\eta}{\eta_m}\right)g(0), \qquad (4.15)
\end{aligned}$$

on using the small-s approximation for $K'(s)$ in the second term in (4.14). In fact, the first term in (4.14) corresponds to the induced velocity in an infinite top-hat cluster and is therefore identically zero, there being no preferred centre of expansion. As anticipated, the induced velocity is inversely proportional to η_m.

The second term on the right-hand side of (4.13) is the additional velocity resulting from the deviation of $g(\eta)$ from $g(0)$, its value at the centre of the cluster, in the interval $(0, \eta)$. The expression (4.13) results in the limit $\eta \ll 1$ from approximating this local deviation by $-c\,\eta^\alpha$ in accordance with (4.11); this is evidently a negative contribution to the induced velocity since the deviation represents a reduction in the number density (contributing to the outward repulsion at η) relative to the leading-order top-hat approximation. The third term in (4.13) is the velocity resulting from the deviation of $g(\eta)$ from the top-hat profile in the interval (η, η_m). Except for the region near η, this deviation may no longer be approximated by (4.11). Thus, this term includes both a local contribution from a region near but outside the interval $(0, \eta)$, and an additional non-local contribution. In Appendix C, it is shown that

$$\begin{aligned}
\lim_{\eta\ll1}\int_{\frac{\eta}{\eta_m}}^1\mathrm{d}s\left[g\left(\frac{\eta}{s}\right)-g(0)\right]\frac{K'(s)}{s}&=\frac{\pi}{4}\eta\int_0^{\eta_m}\mathrm{d}w\frac{[g(0)-g(w)]}{w^2}+\frac{\pi}{4}\frac{c\,\eta^\alpha}{(1-\alpha)}\\
&\quad+c\,\eta^\alpha\int_0^1\mathrm{d}s\frac{1}{s^{1+\alpha}}\left(K'(s)-\frac{\pi}{4}s\right), \qquad (4.16)
\end{aligned}$$

where the integral involving $K'(s)$ is convergent provided $\alpha < 3$. Using (4.16) and (4.15) in (4.13), the original integral equation reduces to

$$\eta\left(\frac{\pi}{4}\frac{g(0)}{\eta_m}+\frac{\pi}{4}\int_0^{\eta_m}\mathrm{d}w\frac{[g(0)-g(w)]}{w^2}\right)+c\,\eta^{\alpha}\left[-\int_0^1 s^{1+\alpha}[K(s)+sK'(s)]\,\mathrm{d}s\right.$$
$$\left.+\frac{\pi}{4(1-\alpha)}+\int_0^1\mathrm{d}s\frac{1}{s^{1+\alpha}}\left(K'(s)-\frac{\pi}{4}s\right)\right]=\frac{\eta}{3} \quad (4.17)$$

in the limit $\eta \ll 1$. The $O(\eta^{\alpha})$ local contributions and the $O(\eta)$ non-local contributions have now been written separately in (4.17). One evidently requires $\alpha \neq 1$ for the coefficient of the $O(\eta^{\alpha})$ contribution to be finite. Therefore, for (4.17) to hold,

$$-\int_0^1 s^{1+\alpha}[K(s)+sK'(s)]\,\mathrm{d}s+\frac{\pi}{4(1-\alpha)}+\int_0^1\mathrm{d}s\frac{1}{s^{1+\alpha}}\left(K'(s)-\frac{\pi}{4}s\right)=0, \quad (4.18)$$

which determines α. It may easily be shown using standard identities involving elliptic functions (for instance, see Gradshteyn & Ryzhik (1965)) that (4.18) is satisfied for $\alpha = 2$. From (4.11), we observe

$$\lim_{\eta\ll 1} g(\eta) = g(0) - c\,\eta^2,$$

so the number density profile has a local maxima at $\eta = 0$ with a finite curvature proportional to c.

In addition, the above implies

$$\frac{\pi}{4}\frac{g(0)}{\eta_m}+\frac{\pi}{4}\int_0^{\eta_m}\mathrm{d}w\frac{[g(0)-g(w)]}{w^2}=\frac{1}{3}, \quad (4.19)$$

so the self-similar expansion of the sedimenting cluster requires that the contributions to the induced velocity near its centre be 'purely non-local'. The requirement that the cluster velocity be linear in the similarity variable has the consequence that the expression

$$\eta\left(\frac{\pi}{4}\frac{g(0)}{\eta_m}+\frac{\pi}{4}\int_0^{\eta_m}\mathrm{d}w\frac{[g(0)-g(w)]}{w^2}\right) \quad (4.20)$$

for the cluster velocity, derived above in the limit $\eta \ll 1$ is, in fact, exact! In other words, (4.20) is the induced velocity for any $\eta < \eta_m$. That the dependence of the induced velocity on $g(\eta)$ is identical for all points in the planar cluster again emphasizes the non-local nature of the underlying hydrodynamic interactions.

4.3. *Cluster size and number density profile*

Using the exact solution, (4.9), in (4.19), we obtain:

$$\frac{\pi}{4}\frac{g(0)}{\eta_m}+\frac{\pi}{4}g(0)\int_0^{\eta_m}\frac{\mathrm{d}w}{w^2}\left[1-\left(1-\frac{w^2}{\eta_m^2}\right)^{\frac{1}{2}}\right]=\frac{1}{3}. \quad (4.21)$$

Note that the left-hand side of (4.21) is the exact expression for the induced velocity derived in the previous section, namely (4.20). The integration in (4.21) is readily performed to yield one relation,

$$g(0)=\frac{8}{3\pi^2}\eta_m, \quad (4.22)$$

between the number density (renormalized in similarity variables) at the centre of the cluster, $\eta = 0$, and the size of the cluster. The other relation, needed to determine $g(0)$ and η_m, is, of course, obtained from the constancy of the total number of particles, that is, from

$$2\pi \int_0^{R_{cl}(t)} n(r, t) r \, \mathrm{d}r = N, \tag{4.23}$$

where $R_{cl}(t) = \eta_m [(Qt)/2\pi]^{1/3}$ is the dimensional radius of the expanding cluster. In dimensionless terms, this becomes

$$2\pi \int_0^{\eta_m} g(\eta) \eta \, \mathrm{d}\eta = N. \tag{4.24}$$

Using the exact solution in (4.24), one obtains the required second relation between $g(0)$ and η_m:

$$g(0) = \frac{3N}{2\pi} \frac{1}{\eta_m^2}. \tag{4.25}$$

From (4.22) and (4.25), we obtain

$$g(0) = \left(\frac{32N}{3\pi^5} \right)^{1/3}, \tag{4.26}$$

$$\eta_m = \left(\frac{9\pi N}{16} \right)^{1/3}. \tag{4.27}$$

Therefore, $n(r, t) \sim O(N^{1/3}/(Qt)^{2/3})$, and the radius of the expanding cluster is given by

$$R_{cl}(t) = \eta_m [Qt/(2\pi)]^{1/3} \tag{4.28}$$

$$= 0.655(NQt)^{1/3} \tag{4.29}$$

$$= 1.743(Nva)^{1/3} t^{1/3}. \tag{4.30}$$

Similar to the spherical cluster, the dilute planar cluster also undergoes a slow self-similar expansion at small Re.

Using (4.26) and (4.27), the exact solution of (4.8) is given by

$$g(\eta) = \left(\frac{32N}{3\pi^5} \right)^{1/3} \left(1 - \frac{(16)^{2/3} \eta^2}{(9\pi N)^{2/3}} \right)^{1/2}. \tag{4.31}$$

Thus, the areal number density profile is locally parabolic near the centre, but is non-analytic near the edge ($\eta = \eta_m$) of the expanding cluster. The non-analyticity implies that $\mathrm{d}g/\mathrm{d}\eta$ diverges as $\eta \to \eta_m$, and is indicative of the steepness of the number density profile at $\eta = \eta_m$.

For a planar cluster, the cluster variance defined in § 3 accounts for the non-uniformity in the areal number density, and may be calculated as

$$\langle r^2 \rangle = \frac{\displaystyle\int_0^{R_{cl}(t)} [r^2 n(r, t)] r \, \mathrm{d}r}{\displaystyle\int_0^{R_{cl}(t)} n(r, t) r \, \mathrm{d}r}, \tag{4.32}$$

and in terms of similarity variables,

$$\langle r^2\rangle = \frac{1}{N}\int_0^{\eta_m}\left[\frac{2\pi}{(Qt)}\right]^{2/3} g(\eta)\left(\frac{\eta(Qt)^{1/3}}{(2\pi)^{1/3}}\right)^3 \mathrm{d}\left(\frac{\eta(Qt)^{1/3}}{(2\pi)^{1/3}}\right)$$

$$= \frac{(2\pi Qt)^{2/3}}{N}\int_0^{\eta_m} g(\eta)\eta^3\,\mathrm{d}\eta$$

$$= \frac{2}{15}\frac{(2\pi)^{2/3}}{N} g(0)\eta_m^4 (Qt)^{2/3}$$

$$= 0.3168\,(Qt)^{2/3}N^{2/3}, \tag{4.33}$$

on using (4.31). Finally, with $Q = 6\pi\nu a$ (see § 2), the variance of the particle positions takes the form

$$\langle r^2\rangle = 2.244(\nu a)^{2/3}N^{2/3}t^{2/3}. \tag{4.34}$$

5. Numerical solution of the initial value problem for a planar cluster

Here, we present a numerical solution of an initial value problem which confirms the theoretical predictions for an axisymmetric planar cluster in the previous section; the inhomogeneous areal number density field offers a better test for the numerics. We do not attempt a comprehensive numerical analysis; rather, the governing equations are solved for a single canonical initial condition, an initial Gaussian profile for the particle number density. Nevertheless, as will be seen, the collapse of the number density profiles at various times, when plotted in appropriate re-scaled coordinates, is strongly suggestive of a self-similar expansion regime in the limit of long times. In addition, the asymptotic forms, close to the centre and edge of the cluster, of the re-scaled number density profiles for long times are consistent with those found in § 4.2 and in Appendix B, respectively.

As in § 2, the governing equation for the number density is given by

$$\frac{\partial n}{\partial t} + \frac{1}{r}\frac{\partial}{\partial r}(ru_r n) = 0, \tag{5.1}$$

where we have assumed axisymmetry; $u_r[n(r,t)]$ is, of course, the radial component of the induced velocity on account of interparticle interactions, and is again a function of $n(r,t)$, this being the origin of the nonlinearity. Equation (5.1) may be written as

$$\frac{\partial n}{\partial t} + u_r\frac{\partial n}{\partial r} = -\left(\frac{\partial u_r}{\partial r} + \frac{u_r}{r}\right)n \tag{5.2}$$

and is a first-order hyperbolic equation. The temporal evolution of the number density profiles may therefore be obtained by integrating along its characteristics, given by $r(t) = \int_0^t u_r[n(r',t')]\,\mathrm{d}t'$. Using (4.1), and a change of variables, the radial velocity may be expressed in the form

$$u_r = \frac{Q}{2\pi}\int_0^1 \mathrm{d}s\left[sK(s)n(rs,t) + K'(s)\left(s^2 n(rs,t) - \frac{n(r/s,t)}{s}\right)\right]. \tag{5.3}$$

Now, using (5.3) in (5.2), we need to integrate the following system of equations:

$$\frac{\mathrm{d}r}{\mathrm{d}t} = \frac{Q}{2\pi}\int_0^1 \mathrm{d}s\left[sK(s)n[r(t)s,t] + K'(s)\left(s^2 n[r(t)s,t] - \frac{n[r(t)/s,t]}{s}\right)\right], \tag{5.4}$$

$$\frac{\mathrm{d}n}{\mathrm{d}t} = \left(\frac{Q}{2\pi}\right) n\int_0^1 \mathrm{d}s\left[K'(s)\left\{\frac{n[r(t)/s,t]/r + n'[r(t)/s,t]/s}{s} - s^2\left(\frac{n[r(t)s,t]}{r} + sn'[r(t)s,t]\right)\right\} - sK(s)\left(\frac{n[r(t)s,t]}{s} + sn'[r(t)s,t]\right)\right]. \tag{5.5}$$

The first equation represents the motion of a Lagrangian point $r(t)$ along the characteristic of (5.2) with a velocity given by (5.3), while the second describes the temporal evolution of the number density at this propagating point. It is convenient at this point to define dimensionless variables. We choose the initial radius of the cluster, characterized by the variance of the initial number density profile, $\langle r_0^2\rangle^{1/2}$, as the length scale. The corresponding time scale is then given by $(\langle r_0^2\rangle^{3/2}/Q)$, and the resulting scale for the velocity field is $(Q/\langle r_0^2\rangle)$. In addition, we use $(N/\pi\langle r_0^2\rangle)$ as the scale for the areal number density field, where $N = 2\pi\int rn(r,t)\mathrm{d}r$ is now the (constant) area under the evolving number density profile; the resulting non-dimensional system of equations is

$$\frac{\mathrm{d}r}{\mathrm{d}t} = \left(\frac{N}{\pi}\right)\int_0^1 \mathrm{d}s\left[sK(s)n[r(t)s,t] + K'(s)\left(s^2 n[r(t)s,t] - \frac{n[r(t)/s,t]}{s}\right)\right], \tag{5.6}$$

$$\frac{\mathrm{d}n}{\mathrm{d}t} = \left(\frac{N}{\pi}\right) n\int_0^1 \mathrm{d}s\left[K'(s)\left\{\frac{n[r(t)/s,t]/r + n'[r(t)/s,t]/s}{s} - s^2\left(\frac{n[r(t)s,t]}{r} + sn'[r(t)s,t]\right)\right\} - sK(s)\left(\frac{n[r(t)s,t]}{s} + sn'[r(t)s,t]\right)\right], \tag{5.7}$$

where we continue to use the same symbols for the dimensionless variables in the interests of notational simplicity. The expression for the variance in the self-similar regime derived earlier, (4.33), may now be written in the form $\langle r^2\rangle = 0.3168N^{2/3}t^{2/3}$ in terms of the dimensionless variables defined above. Clearly, one expects the sedimenting cluster to asymptote to a self-similar expansion only in the limit when its radius $(\langle r^2\rangle^{1/2})$ at time t becomes much larger than the initial value $(\langle r_0^2\rangle^{1/2})$, so the latter ceases to be a relevant length scale. Thus, N may be regarded as a parameter that determines the duration of time required for an evolving cluster to cross over to the self-similar regime.

The inverse dependence on r in the above equations, however, makes numerical integration difficult for points close to the centre of the cluster. We therefore combine (5.6) and (5.7) with suitably simplified limiting forms for small r, which is convenient for Lagrangian points close to the centre ($r = 0$); from symmetry, the centre of the cluster remains a Lagrangian point for all times. The asymptotic form of (5.6) for $r \to 0$ has already been derived in § 4.2, being given by (4.20), and the near-field form of (5.7) may be derived similarly. The simplified system of equations, used in the limit of small r, is given by

$$\lim_{r\to 0}\frac{\mathrm{d}r}{\mathrm{d}t} = \left(\frac{N}{\pi}\right)\frac{\pi}{4}r\left[\int_0^\infty \mathrm{d}s\,\frac{[n(0,t) - n(s,t)]}{s^2}\right], \tag{5.8}$$

$$\lim_{r\to 0}\frac{\mathrm{d}n}{\mathrm{d}t} = \left(\frac{N}{\pi}\right)\frac{\pi}{4}n\left[\int_0^\infty \mathrm{d}s\,\frac{n'(s,t)}{s} - \int_0^\infty \mathrm{d}s\,\frac{[n(0,t) - n(s,t)]}{s^2}\right]. \tag{5.9}$$

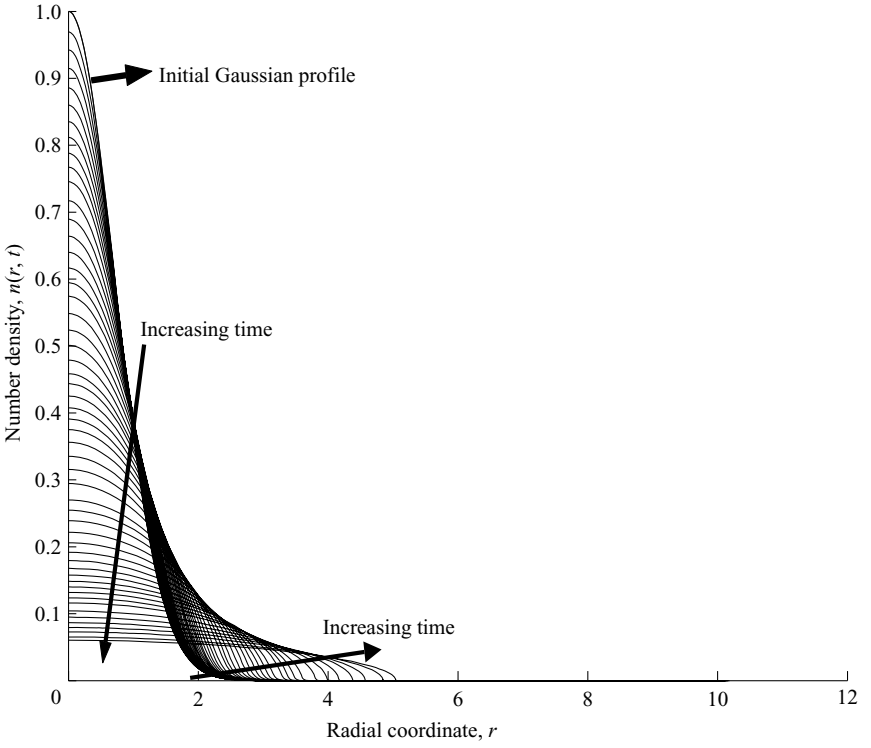

FIGURE 4. The number density profiles at various instants of time from $t = 0$ to $t \approx 44.3$, where the time is in units of $(\langle r_0^2 \rangle^{3/2}/Q)$; the number density field is a Gaussian at $t = 0$.

The numerical integration was performed using an adaptive step Runge–Kutta routine. The integration was begun with 800 evenly spaced points in the interval $r \in [0, 10]$, the initial value of the number density at each of these points being that of a Gaussian profile, namely $e^{-x_i^2}$ $(N = \pi)$; x_i here denotes the ith Lagrangian point. The variance of the initial Gaussian profile was 0.5, while the variance of the number density profile at the final time step ($t \approx 44.3$) is approximately 5; the aforementioned radial interval is therefore sufficient in extent to accurately represent the evolution of the initial profile for the range of times integrated. At every time step, one needs the current value of the number density and its spatial gradient at the current location of each Lagrangian point in order to predict the new values. These were obtained from a linear interpolation between the values at the previous locations of the Lagrangian points. Also, the values of the elliptic function $K(s)$ and its derivative, required for the evaluation of the integrals in (5.6) and (5.7), may be obtained from standard series formulations (for instance, see Gradshteyn & Ryzhik 1965). The integrals themselves were evaluated using Legendre quadrature with 500 quadrature points. As a check on numerical accuracy, the value of $\int n(r, t) r \mathrm{d}r$ was monitored at every time step, and was found to remain virtually unchanged during the time interval of integration; this, of course, must be so, since the total number of particles is conserved.

Figure 4 depicts the evolution of the number density field with time starting from an initial Gaussian profile. The profiles become progressively flatter at the centre, and steeper toward the edge of the cluster. The analysis in §4 suggests that the sedimenting cluster must approach a self-similar expansion only in the limit of long times, when the details of the initial condition are forgotten. Thus, if the proposed

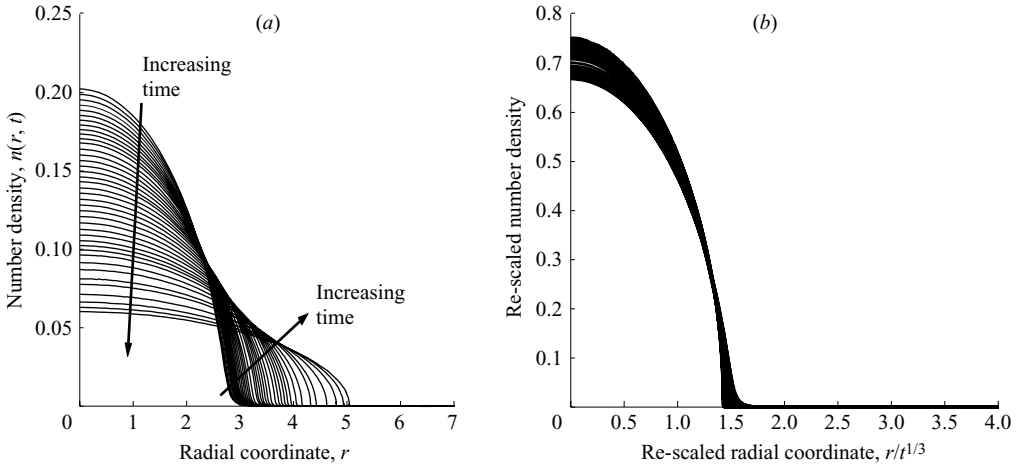

FIGURE 5. (*a*) Plots of $n(r, t)$ as a function of r for $t > 6$, and (*b*) a plot of the re-scaled number density field $t^{2/3}n(r, t)$ as a function of the similarity variable $\eta \equiv r/t^{1/3}$.

self-similar regime indeed exists, the profiles of the number density when plotted in appropriate re-scaled variables, namely $n(r, t)t^{2/3}$ versus $r/t^{1/3}$, must collapse onto a single universal curve for sufficiently long times. This is seen in figure 5, where the number density profiles are plotted as a function of the radial coordinate in both the scaled and unscaled forms for $t > 6$; that the similarity scaling works is evident. Figure 6 is a plot of $\{n(0, t_f) - n(r, t_f)\}$ as a function of r, for small r, on a log-log scale, while figure 7 is a log-log plot of $n(r, t_f)$ versus $(r_m - r)$; here, $n(r, t_f)$ is the number density profile at the final time step, $t_f \approx 44.3$, and r_m denotes the location of the cluster edge at this time. Since the number density profiles have increasingly steep rims for long times, the numerical value of r_m in this case is easily inferred by inspection. Together, the plots confirm the limiting forms of the number density profile for $r \to 0$ (locally quadratic) and $r \to r_m$ (singular slope), found in § 4.2 and in Appendix C, respectively. In figure 6, we note that the density of Lagrangian points falls off near the centre of the cluster, since the induced velocity at all locations is directed radially outward and causes these points to concentrate near the edge of the cluster for long times. However, points not too far away from the cluster centre do conform to a local quadratic behaviour, as is evident from a comparison with a straight line of slope 2 also shown in the figure. In figure 7, a favourable comparison with a straight line of slope 0.5 confirms the predicted non-analytic behaviour of the number density for $\to r_m$; note that the accuracy of the numerics drops for points very near the edge of the cluster, as the number density profile here becomes very steep and jagged for long times.

In figure 8, we plot the induced velocity profiles corresponding to the number density profiles shown in figure 4 in both the scaled and unscaled forms. According to the similarity transformation, the number density is $O[t^{-\frac{2}{3}}g(r/t^{1/3})]$ (see § 4.3), and the corresponding induced velocity $u_r(r, t)$ will be $O[t^{-\frac{2}{3}}(r/t^{1/3})]$. Thus, a plot of $u_r(r, t)t^{2/3}$ against $r/t^{1/3}$ should cause the velocity profiles to collapse onto a single universal curve for times when the details of the initial condition are no longer important; this is evident in figure 8(*b*).

We observe that, for the initial Gaussian profile, the induced velocity increases with distance from the centre of the cluster to begin with, since an increasing number of

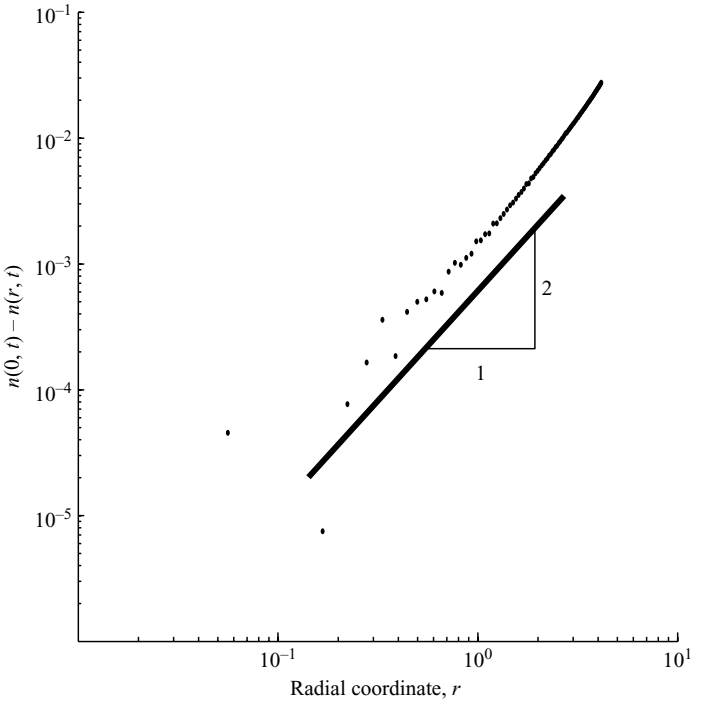

FIGURE 6. The points represent the values of $\{n(0, t) - n(r, t)\}$ for $t = 44.3$, plotted as a function of r, on a logarithmic scale; a straight line with slope 2 corresponding to a parabolic number density profile is shown for comparison.

particles contribute to a radial repulsion. However, beyond a certain critical distance, of the order of the variance of the Gaussian profile, the number density has decreased to substantially smaller values. As a result, there is little change in the number of particles already contributing to an outward repulsion; instead, owing to the decay with distance of the source velocity field associated with any given particle, the repulsion now becomes weaker with increasing distance from the cluster centre. The resulting induced velocity decreases. Thus, the initial profile for the induced velocity exhibits a maximum at an intermediate location ($r \approx 2.5$ in figure 8), implying that particles in this region move outward at a rate faster than particles further out, eventually catching up with them. This leads to an evident steepening of the number density profile with increasing time (see figure 4). Correspondingly, the region where the induced velocity field increases with an increase in distance from the centre becomes larger in extent; in addition, there is a sharper transition between regions of increasing and decreasing induced velocity. Finally, as one approaches the self-similar expansion regime, the number density profile has steepened to an extent, where one may unambiguously identify a 'cluster edge' beyond which the number density reduces to very small values. In turn, this leads to an almost discontinuous transition (a 'kink') from the linearly increasing induced velocity up to the edge of the cluster to a nonlinear decrease in the region beyond it. This prediction is in accordance with theory.

Finally, we plot $\langle r^2 \rangle$ as a function of time. The theory predicts that $\langle r^2 \rangle \propto t^{2/3}$ in the regime of self-similar expansion. For the initial Gaussian profile used in the numerical integration, the coefficient of proportionality is found to be approximately 0.67. In

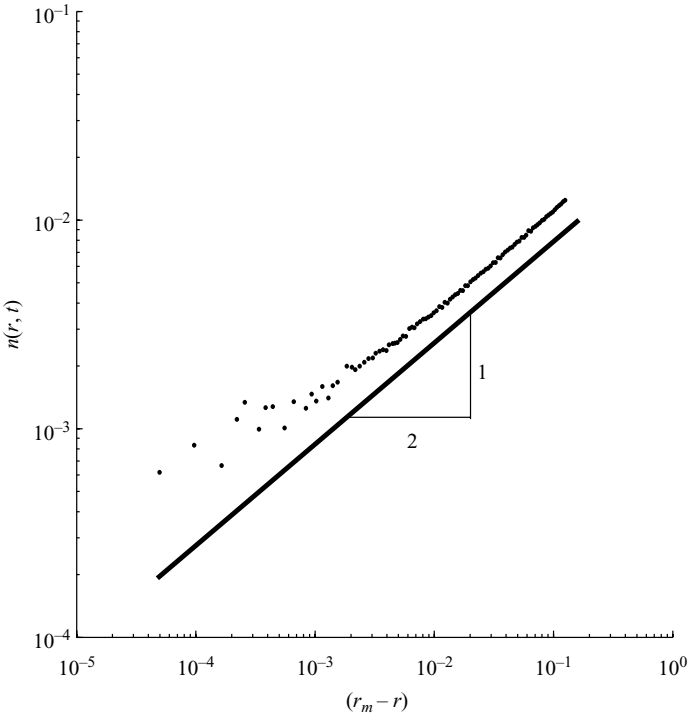

FIGURE 7. The points represent the values of $n(r, t)$ at $t = 44.3$ plotted against $(r_m - r)$, on a logarithmic scale, for values of r close to r_m; here, r_m denotes the edge of the cluster, and is found to approximately equal 5.45 from a visual inspection of the number density profile. The theoretical prediction, a straight line with slope 0.5, is shown for comparison.

figure 9, the curve obtained from the numerical integration appears to asymptote to the theoretical straight line for long times, indicating an approach toward a self-similar expansion. An unambiguous verification of the $O(t^{2/3})$ scaling for the variance would require the numerical integration to be carried out for still longer times. However, as mentioned earlier, the increased steepness of the number density profile at the edge of the cluster makes this unfeasible. The rapid changes in the number density in this region limit numerical accuracy, causing the profile to become jagged for $t > 44$, and the numerical integration becomes extremely time consuming; the integration was therefore terminated at $t \approx 44.3$. This may also account for appearance of ripples in the plot in figure 9 at long times. It must be emphasized, however, that, despite the plot of the variance of the particle positions being inconclusive in itself, all remaining cluster characteristics are consistent with the theoretical predictions.

6. Discussion and conclusion

The theoretical analysis presented should be taken as a step towards a mechanistic understanding of finite-*Re* hydrodynamic interactions between sedimenting particles. Dilute spherical and planar clusters, dominated by source–field interactions, present analytically tractable situations in this regard; in addition, as discussed in § 2, they also appear to be relevant long-time scenarios. It would be of interest to extend the analysis to study the more difficult problem concerning the evolution of sufficiently dense sedimenting blobs where wake interactions come into play, and persist for the

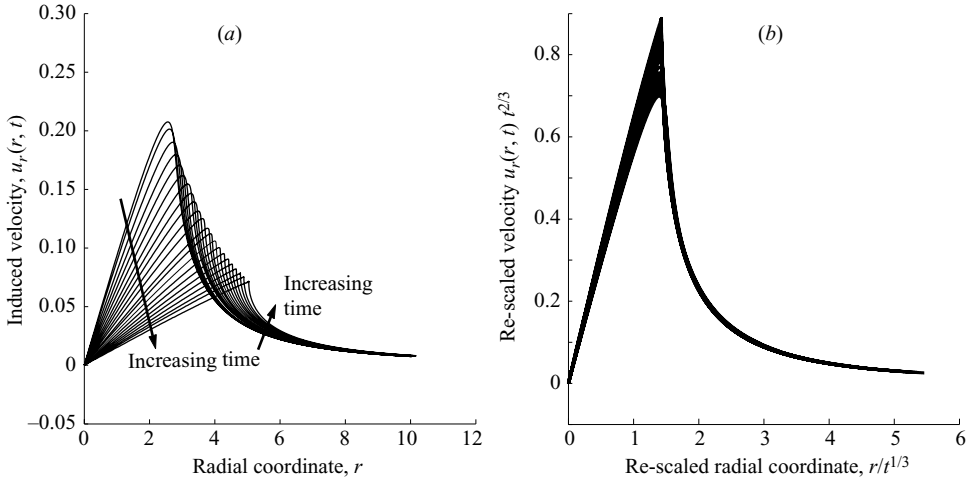

FIGURE 8. (*a*) The evolution of $u_r(r,t)$ as a function of r starting from a Gaussian initial condition. (*b*) A plot of $u_r(r,t)t^{2/3}$ versus $r/t^{1/3}$ for times $t > 6$, confirming the presence of a long-time self-similar expansion regime.

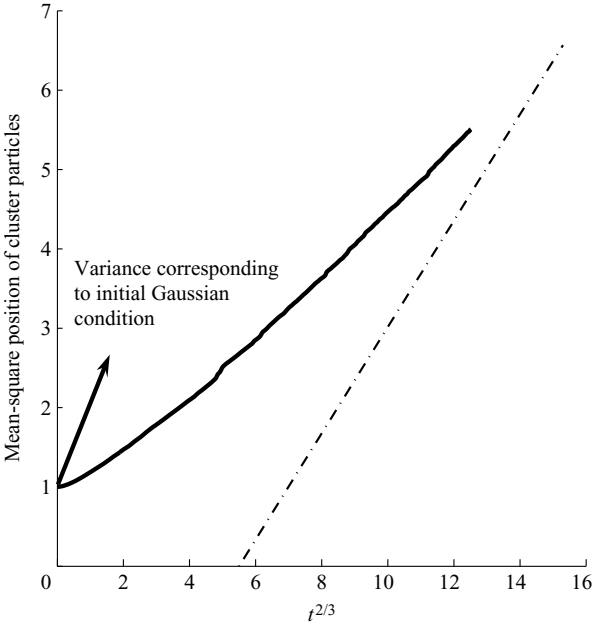

FIGURE 9. The plot of $\langle r^2 \rangle$, the mean-square position of the cluster particles, as a function of $t^{2/3}$. For the parameters used in the numerical integration, the theoretical prediction for a self-similarly expanding cluster is a straight line (dash-dot line) with a slope of 0.67.

entire duration of cluster evolution. Simulations may play an invaluable role in this regard. Along the lines of Machu *et al.*(2001), one may perform 'Oseenlet simulations' wherein the velocity disturbance due to each sedimenting particle is taken to be the Oseen velocity field, a uniformly valid approximation for small *Re*. With the dynamics thus specified, the simulation, at each time step, would simply proceed by an update of the particle positions in accordance with the values of the velocity field at their

respective centres. The induced velocity field at the centre of any given particle is equal to the sum of the (Oseen) velocity disturbances due to all other particles. Such a kinematic simulation, of course, needs only a fraction of the computational power required for a full dynamic simulation of the Navier–Stokes equations at any finite Re using any of the standard protocols, say, the lattice Boltzmann technique, finite element methods, etc. However, even with the simplistic underlying physics, kinematic simulations are expected to yield useful insights into the dynamics of large sedimenting blobs in the dilute limit.

A kinematic simulation of a dilute suspension jet, for instance, might help account for some recent observations by Nicolas (2002) in his experiments involving gravity-driven dense suspension jets. Of particular interest was the change in the behaviour of the suspension jet for $Re > O(1)$, Re again being the Reynolds number based on the particle size and settling velocity. The jet was found to remain uniformly cylindrical at vanishingly small Re, and then, at slightly higher Re, underwent an apparent instability, leading to formation of discrete blobs. Further, for $Re > 1$, the particulate jet began to disperse. This dispersion, and the resulting rapid expansion in the longitudinal direction, apparently triggered when micro-scale inertial forces first become important, may be related to the interparticle repulsion mechanism analysed in this paper. Such a simulation may also be used to probe aspects of the tentative phase diagram for inertial clusters sketched out in figure 1; in particular, one may look at transitions across boundaries demarcating different dynamical behaviour, provided the simulations include the underlying physics in all the relevant bounding regimes. Even for the case of sedimenting clusters dominated by source–field interactions, it would be of interest to verify if the cluster evolves towards the axisymmetric self-similar expansion regime even in the presence of initial non-axisymmetric perturbations.

This work was supported by NSF grant CBET-0730579.

Appendix A. Exact solution of the integral equation (4.8)

Here, we show that $g(\eta) = C(1 - \eta^2/\eta_m^2)^{1/2}$ exactly satisfies (4.8). Equation (4.8) being linear, the constant C is arbitrary. For our problem, however, $g(\eta)$ is the number density field in similarity variables, and C is therefore related to η_m via the normalization condition. We proceed by showing that substitution of the above expression for $g(\eta)$ in (4.8) leads to an identity. Using (4.10), obtained from (4.8) after a change of variables, it is then required to prove

$$\int_0^1 s[K(s) + sK'(s)](1 - \hat{\eta}^2 s^2)^{1/2}\,\mathrm{d}s - \int_{\hat{\eta}}^1 \frac{K'(s)}{s}\left(1 - \frac{\hat{\eta}^2}{s^2}\right)^{\frac{1}{2}}\,\mathrm{d}s = 0. \tag{A 1}$$

with $\hat{\eta} = \eta/\eta_m$, so $0 \leqslant \hat{\eta} \leqslant 1$.

The left-hand side of (A 1), after a slight rearrangement, yields

$$\begin{aligned}
&\int_0^1 \left[s\left\{K(s) + sK'(s)\right\} - \frac{K'(s)}{s}\right]\mathrm{d}s + \int_0^{\hat{\eta}} \frac{K'(s)}{s}\,\mathrm{d}s \\
&\quad - \sum_{n=1}^{\infty} \frac{1\cdot 1\cdot 3\ldots(2n-3)}{2\cdot 4\ldots(2n)}\,\hat{\eta}^{2n} \int_0^1 s^{2n+1}[K(s) + sK'(s)]\,\mathrm{d}s \\
&\quad + \int_{\hat{\eta}}^1 \frac{K'(s)}{s}\left[1 - \left(1 - \frac{\hat{\eta}^2}{s^2}\right)^{1/2}\right]\mathrm{d}s,
\end{aligned} \tag{A 2}$$

where we have used the binomial series expansion of $(1-\hat{\eta}^2 s^2)^{1/2}$ in the first term in (A 1). The first term in (A 2) is proportional to the induced velocity in an infinite top-hat cluster, and is therefore zero by symmetry. Using the known series expansion for the elliptic function $K(s)$, $K(s)=\sum_{n=0} a_n s^{2n}$, we have $K'(s)=\sum_{n=0}^{\infty} b_n s^{2n+1}$ where $b_n=(2n+1)a_{n+1}$ (see Gradshteyn & Ryzhik (1965)). Therefore, (A 2) may be written as

$$\sum_{n=0}^{\infty}\frac{b_n}{2n+1}\hat{\eta}^{2n+1}-\sum_{n=1}^{\infty}\frac{1\cdot1\cdot3\ldots(2n-3)}{2\cdot4\ldots(2n)}\hat{\eta}^{2n}\int_0^1 s^{2n+1}[K(s)+sK'(s)]\,\mathrm{d}s$$
$$+b_0\sum_{n=1}^{\infty}\frac{1\cdot1\cdot3\ldots(2n-3)}{2\cdot4\ldots(2n)}\int_{\hat{\eta}}^1\frac{\hat{\eta}^{2n}}{s^{2n}}\,\mathrm{d}s+\int_{\hat{\eta}}^1\frac{[K'(s)-b_0 s]}{s}\left[1-\left(1-\frac{\hat{\eta}^2}{s^2}\right)^{1/2}\right]\mathrm{d}s, \tag{A 3}$$

where we have again used the binomial series expansion for $[1-(1-\hat{\eta}^2/s^2)^{1/2}]$. Evaluating the coefficient of b_0 in the third term, we obtain

$$\sum_{n=0}^{\infty}\frac{b_n}{2n+1}\hat{\eta}^{2n+1}-\sum_{n=1}^{\infty}\frac{1\cdot1\cdot3\ldots(2n-3)}{2\cdot4\ldots(2n)}\hat{\eta}^{2n}\int_0^1 s^{2n+1}[K(s)+sK'(s)]\,\mathrm{d}s$$
$$+b_0\hat{\eta}\sum_{n=1}^{\infty}\frac{1\cdot1\cdot3\ldots(2n-3)}{2\cdot4\ldots(2n)}\frac{1}{(2n-1)}-b_0\sum_{n=1}^{\infty}\frac{1\cdot1\cdot3\ldots(2n-3)}{2\cdot4\ldots(2n)}\frac{\hat{\eta}^{2n}}{(2n-1)}$$
$$+\int_{\hat{\eta}}^1\frac{[K'(s)-b_0 s]}{s}\left[1-\left(1-\frac{\hat{\eta}^2}{s^2}\right)^{\frac{1}{2}}\right]\mathrm{d}s. \tag{A 4}$$

Since $[1-(1-\hat{\eta}^2/s^2)^{1/2}]\sim O(\hat{\eta}^2)$ for $s\sim O(1)$, and $[K'(s)-b_0 s]/s\sim b_1\hat{\eta}^2$ for $s\sim O(\hat{\eta})$, the integrand in the last term in (A 4) remains $O(\hat{\eta}^2)$ for all s. Thus, the second and fourth summations, and the last term in (A 4), are all $O(\hat{\eta}^2)$; their neglect yields the induced velocity in the cluster correct to $O(\hat{\eta})$. This was, of course, determined earlier when evaluating the number density profile near the centre of the cluster, and corresponds to the first term in (4.17).

More importantly, the above procedure may now be carried out in a systematic manner to higher orders, and (A 2) may thus be ordered as an infinite series in powers of $\hat{\eta}$. For instance, at the next order, we obtain

$$\sum_{n=0}^{\infty}\frac{b_n}{2n+1}\hat{\eta}^{2n+1}-\sum_{n=1}^{\infty}\frac{1\cdot1\cdot3\ldots(2n-3)}{2\cdot4\ldots(2n)}\hat{\eta}^{2n}\int_0^1 s^{2n+1}[K(s)+sK'(s)]\,\mathrm{d}s$$
$$+b_0\hat{\eta}\sum_{n=1}^{\infty}\frac{1\cdot1\cdot3\ldots(2n-3)}{2\cdot4\ldots(2n)}\frac{1}{(2n-1)}-b_0\sum_{n=1}^{\infty}\frac{1\cdot1\cdot3\ldots(2n-3)}{2\cdot4\ldots(2n)}\frac{\hat{\eta}^{2n}}{(2n-1)}$$
$$+\frac{\hat{\eta}^2}{2}\int_0^1\frac{[K'(s)-b_0 s]}{s^3}\,\mathrm{d}s-\frac{\hat{\eta}^2}{2}\sum_{n=0}^{\infty}\frac{b_{n+1}}{2n+1}\hat{\eta}^{2n+1}$$
$$+b_1\hat{\eta}^3\sum_{n=2}^{\infty}\frac{1\cdot1\cdot3\ldots(2n-3)}{2\cdot4\ldots(2n)}\frac{1}{(2n-3)}-b_1\sum_{n=2}^{\infty}\frac{1\cdot1\cdot3\ldots(2n-3)}{2\cdot4\ldots(2n)}\frac{\hat{\eta}^{2n}}{(2n-3)}$$
$$+\int_{\hat{\eta}}^1\frac{[K'(s)-b_0 s-b_1 s^3]}{s}\left[1-\left(1-\frac{\hat{\eta}^2}{s^2}\right)^{\frac{1}{2}}-\frac{\hat{\eta}^2}{2s^2}\right]\mathrm{d}s, \tag{A 5}$$

where the last integral is $O(\hat{\eta}^4)$.

The complete power series may be written in the form

$$\sum_{n=0}^{\infty}\frac{b_n}{2n+1}\,\hat{\eta}^{2n+1}-\sum_{n=1}^{\infty}\frac{1\cdot1\cdot3\ldots(2n-3)}{2\cdot4\ldots(2n)}\,\hat{\eta}^{2n}\int_0^1 s^{2n+1}[K(s)+sK'(s)]\,\mathrm{d}s$$
$$+b_0\hat{\eta}\sum_{n=1}^{\infty}\frac{1\cdot1\cdot3\ldots(2n-3)}{2\cdot4\ldots(2n)}\frac{1}{(2n-1)}-b_0\sum_{n=1}^{\infty}\frac{1\cdot1\cdot3\ldots(2n-3)}{2\cdot4\ldots(2n)}\frac{\hat{\eta}^{2n}}{(2n-1)}$$
$$+\frac{\hat{\eta}^2}{2}\int_0^1\frac{[K'(s)-b_0s]}{s^3}\,\mathrm{d}s-\frac{\hat{\eta}^2}{2}\sum_{n=0}^{\infty}\frac{b_{n+1}}{2n+1}\,\hat{\eta}^{2n+1}$$
$$+b_1\hat{\eta}^3\sum_{n=2}^{\infty}\frac{1\cdot1\cdot3\ldots(2n-3)}{2\cdot4\ldots(2n)}\frac{1}{(2n-3)}-b_1\sum_{n=2}^{\infty}\frac{1\cdot1\cdot3\ldots(2n-3)}{2\cdot4\ldots(2n)}\frac{\hat{\eta}^{2n}}{(2n-3)}+\cdots$$
$$+b_k\hat{\eta}^{2k+1}\sum_{n=k+1}^{\infty}\frac{1\cdot1\cdot3\ldots(2n-3)}{2\cdot4\ldots(2n)}\frac{1}{(2n-2k-1)}$$
$$-b_k\sum_{n=k+1}^{\infty}\frac{1\cdot1\cdot3\ldots(2n-3)}{2\cdot4\ldots(2n)}\frac{\hat{\eta}^{2n}}{(2n-2k-1)}$$
$$+\frac{1\cdot1\cdot3\ldots(2k-1)}{2\cdot4\ldots(2k+2)}\,\hat{\eta}^{2k+2}\int_0^1\frac{[K'(s)-b_0s-b_1s^3-\cdots-b_ks^{2k+1}]}{s^{2k+3}}\,\mathrm{d}s$$
$$-\frac{1\cdot1\cdot3\ldots(2k-1)}{2\cdot4\ldots(2k+2)}\,\hat{\eta}^{2k+2}\sum_{n=0}^{\infty}\frac{b_{n+k+1}}{2n+1}\,\hat{\eta}^{2n+1}+\cdots. \tag{A 6}$$

Thus, for $g(\eta)=C(1-\hat{\eta}^2)^{1/2}$ to be an exact solution, the individual coefficients in the above infinite series must be zero. For odd exponents ($\hat{\eta}^{2k+1}$), this requirement implies

$$\sum_{n=1}^{\infty}\frac{1\cdot1\cdot3\ldots(2n-3)}{2\cdot4\ldots(2n)}\frac{1}{(2n-2k-1)}=-\frac{1}{(2k+1)}, \tag{A 7}$$

for $k=1,2,\ldots$, an identity which is easily verified numerically. Equating the coefficient of $\hat{\eta}^{2k}$ to zero, one obtains

$$\int_0^1\frac{[K'(s)-b_0s-b_1s^3-\cdots-b_{k-1}s^{2k-1}]}{s^{2k+1}}\,\mathrm{d}s-\frac{b_0}{(2k-1)}-\frac{b_1}{(2k-3)}-\cdots-b_{k-1}$$
$$=\int_0^1 s^{2k+1}[K(s)+sK'(s)]\,\mathrm{d}s, \tag{A 8}$$

for even exponents, or alternatively,

$$\int_0^1\frac{K'(s)}{s^{2k+1}}\,\mathrm{d}s-\lim_{s\to0}\left[\frac{b_0}{(2k-1)s^{2k-1}}+\frac{b_1}{(2k-3)s^{2k-3}}+\cdots+\frac{b_{k-1}}{s}\right]$$
$$=\int_0^1 s^{2k+1}[K(s)+sK'(s)]\,ds, \tag{A 9}$$

where the second term on the left-hand side removes the divergent part of $K'(s)/s^{2k+1}$ when integrated over [0, 1].

We prove (A 9) using the principle of mathematical induction, that is, assume (A 9) to hold for $k=m$, and show the same to be true for $k=m+1$. Thus, one needs to

prove

$$\int_0^1 \frac{K'(s)}{s^{2m+3}}\,\mathrm{d}s - \lim_{s\to 0}\left[\frac{b_0}{(2m+1)s^{2m+1}} + \frac{b_1}{(2m-1)s^{2m-1}} + \cdots + \frac{b_m}{s}\right] = \int_0^1 s^{2m+3}[K(s) + sK'(s)]\,\mathrm{d}s, \quad \text{(A 10)}$$

using (A 9) for $k = m$. We begin by using the following recurrence relation between elliptic functions:

$$\int s^{2m+3}K(s)\,\mathrm{d}s = \frac{4(m+1)^2}{(2m+3)^2}\int s^{2m+1}K(s)\,\mathrm{d}s + \frac{s^{2m+2}}{(2m+3)^2}\left[E(s) - (2m+3)(1-s^2)K(s)\right], \quad \text{(A 11)}$$

where $E(s) = (1-s^2)[sK'(s) + K(s)]$ (see Byrd & Morris 1971). Integrating by parts, and specifying the interval for integration to be [0, 1], we obtain

$$\int_0^1 \frac{K'(s)}{s^{2m+3}}\,\mathrm{d}s = \frac{4(m+1)^2}{(2m+1)(2m+3)}\int_0^1 \frac{K'(s)}{s^{2m+1}}\,\mathrm{d}s - \frac{1}{(2m+3)} - \frac{1}{(2m+1)(2m+3)}\lim_{s\to 1}K(s) + \lim_{s\to 0}\left[\frac{4(m+1)^2}{(2m+1)(2m+3)}\frac{1}{s^{2m+1}} - \frac{1}{s^{2m+3}}\right]K(s) + \lim_{s\to 0}\frac{(1-s^2)}{(2m+3)s^{2m+3}}[sK'(s) + (2m+3)K(s)], \quad \text{(A 12)}$$

where, in the light of (A 9), we have replaced m by $-(m+3)$ in (A 11). Using (A 9) with $k = m$ for the integral on the right-hand side, we obtain

$$\int_0^1 \frac{K'(s)}{s^{2m+3}}\,\mathrm{d}s = \frac{4(m+1)^2}{(2m+1)(2m+3)}\left[\int_0^1 s^{2m+1}[K(s) + sK'(s)]\,\mathrm{d}s + \lim_{s\to 0}\left\{\frac{b_0}{(2m-1)s^{2m-1}} + \frac{b_1}{(2m-3)s^{2m-3}} + \cdots + \frac{b_{m-1}}{s}\right\}\right] + \lim_{s\to 0}\left[\frac{4(m+1)^2}{(2m+1)(2m+3)}\frac{1}{s^{2m+1}} - \frac{1}{s^{2m+3}}\right]K(s) + \lim_{s\to 0}\frac{(1-s^2)}{(2m+3)s^{2m+3}}\left[sK'(s) + (2m+3)K(s)\right]. \quad \text{(A 13)}$$

Now, using (A 11) over [0, 1], and (A 12), we obtain

$$\int_0^1 s^{2m+1}K(s)ds = \frac{(2m+3)^2}{4(m+1)^2}\int_0^1 s^{2m+3}K(s)ds - \frac{1}{4(m+1)^2}, \quad \text{(A 14)}$$

$$\int_0^1 s^{2m+2}K'(s)\,\mathrm{d}s = \frac{(2m+3)^2}{(2m+2)(2m+4)}\int_0^1 s^{2m+4}K'(s)\,\mathrm{d}s - \frac{1}{(2m+2)(2m+4)}\lim_{s\to 1}K(s) + \frac{1}{2(m+1)}. \quad \text{(A 15)}$$

Using (A 14) and (A 15), we have

$$\frac{4(m+1)^2}{(2m+1)(2m+3)}\int_0^1 s^{2m+1}[K(s)+sK'(s)]\mathrm{d}s = \frac{(2m+3)}{(2m+1)}\left[\int_0^1 s^{2m+3}K(s)\,\mathrm{d}s + \frac{(2m+2)}{(2m+4)}\int_0^1 s^{2m+4}K'(s)\,\mathrm{d}s\right] + \frac{1}{(2m+3)} - \frac{(2m+2)}{(2m+1)(2m+3)(2m+4)}\lim_{s\to 1}K(s). \tag{A 16}$$

On integrating by parts, we obtain

$$\frac{4(m+1)^2}{(2m+1)(2m+3)}\int_0^1 s^{2m+1}[K(s)+sK'(s)]\,\mathrm{d}s = \int_0^1 s^{2m+3}[K(s)+sK'(s)]\,\mathrm{d}s + \frac{1}{(2m+3)} + \frac{2(m+2)}{(2m+1)(2m+3)(2m+4)}\lim_{s\to 1}K(s). \tag{A 17}$$

Using (A 17) in (A 13), we obtain after some simplification

$$\int_0^1 \frac{K'(s)}{s^{2m+3}}\,\mathrm{d}s = \int_0^1 s^{2m+3}[K(s)+sK'(s)]\,\mathrm{d}s + \lim_{s\to 0}\frac{1}{(2m+1)(2m+3)}\frac{K(s)}{s^{2m+1}} + \lim_{s\to 0}\frac{1}{(2m+3)}\frac{K'(s)(1-s^2)}{s^{2m+2}} + \frac{4(m+1)^2}{(2m+1)(2m+3)}\lim_{s\to 0}\left[\frac{b_0}{(2m-1)s^{2m-1}} + \frac{b_1}{(2m-3)s^{2m-3}} + \cdots + \frac{b_{m-1}}{s}\right]. \tag{A 18}$$

Using the aforementioned power series for $K(s)$ and $K'(s)$, it may easily be shown, after some algebra involving the a_n and b_n, that (A 18) reduces to (A 10). Now, it only remains to show (A 9) for $k=1$, whence it would follow for all positive k, thereby completing the proof; the equality for $k=1$ may easily be shown using standard relations involving elliptic functions (for instance, see Gradshteyn & Ryzhik 1965; Byrd & Morris 1971).

Appendix B. The number density profile near the edge of a planar sedimenting cluster

According to (4.8), for $\eta \to \eta_{m-}$, the induced cluster velocity, expressed in similarity variables, must tend to a finite value, proportional to $\eta_m/3$, at the edge of the cluster, with a finite positive slope. It is shown here that these twin constraints completely specify the asymptotic form of $g(\eta)$ near the cluster edge. For $\eta > \eta_m$, $g(\eta)$ is, of course, identically zero, the cluster being finite in extent. This kink in the number density profile introduces a corresponding kink in the profile for the induced velocity at the cluster edge ($\eta = \eta_m$). On one hand, the induced velocity must increase linearly with η for $\eta < \eta_m$, and on the other, it must decrease for $\eta > \eta_m$, approaching zero for $\eta \to \infty$, as the repelling particles in the sedimenting cluster move further away.

Differentiating (4.8) with respect to η, we obtain, notwithstanding multiplicative factors of t, the following expression for the rate of increase of the induced velocity

U^i_{cl} with η:

$$\frac{\mathrm{d}U^i_{cl}}{\mathrm{d}\eta} = \int_0^1 s^2[K(s) + sK'(s)]g'(\eta s)\,\mathrm{d}s - \int_{\eta/\eta_m}^1 \frac{K'(s)}{s^2}\, g'\left(\frac{\eta}{s}\right)\,\mathrm{d}s, \tag{B 1}$$

where the prime denotes differentiation, and we have used $g(\eta_m) = 0$. We rewrite (B 1) in the form

$$\frac{\mathrm{d}U^i_{cl}}{\mathrm{d}\eta} = \int_0^1 s^2K(s)g'(\eta s)\,\mathrm{d}s + \int_0^{\eta/\eta_m} s^3K'(s)g'(\eta s)\,\mathrm{d}s + \int_{\eta/\eta_m}^1 K'(s)\left[s^3g'(\eta s) - \frac{1}{s^2}\, g'\left(\frac{\eta}{s}\right)\right]\mathrm{d}s. \tag{B 2}$$

For $g'(\eta_m)$ finite and negative, the integrand in the third term remains finite since the singularity of $K'(s)$ is now offset by the factor $(s^3 - 1/s^2)$ for $s \to 1$; this term therefore tends to zero as $\eta \to \eta_m$. Since the first term in (B 2) remains finite in this limit, we have

$$\lim_{\eta\to\eta_m} \frac{\mathrm{d}U^i_{cl}}{\mathrm{d}\eta} \approx \lim_{\eta/\eta_m\to 1} \int_0^{\eta/\eta_m} \frac{g'(\eta_m s)}{2(1-s)}\,\mathrm{d}s, \tag{B 3}$$

where we have used the asymptotic form of $K'(s)$ for $s \to 1$ (see Gradshteyn & Ryzhik 1965). Thus, $\mathrm{d}U^i_{cl}/\mathrm{d}\eta$ diverges logarithmically for $\eta \to \eta_m$. Physically, the contribution to the induced velocity at any point within the cluster is dominated by the repulsive interaction velocities due to particles at distances of the order of the cluster size. As the point moves towards the cluster edge, the number density in its vicinity starts to decrease; the repelling particles move further away on average, and this decrease in the magnitude of repulsion is not compensated by a corresponding increase in their number. The induced velocity therefore starts to decrease; it attains a maximum for $\eta < \eta_m$, and decreases thereafter, approaching $\eta = \eta_m$ with an infinite negative slope. For increasingly flatter number density profiles (with correspondingly steeper rims), the location of the maximum in the induced velocity approaches η_m, and the turnover of the induced velocity close to the cluster edge becomes progressively sharper. Evidently, number density profiles that asymptote to a finite slope at $\eta = \eta_m$ cannot be solutions of (4.8).

We now show that the number density profile must necessarily have the asymptotic form $\lim_{\eta\to\eta_m} g(\eta) \approx (1-\eta/\eta_m)^{1/2}$, for $\mathrm{d}U^i_{cl}/\mathrm{d}\eta|_{\eta=\eta_m}$ to be finite. To this end, we denote the indefinite integrals of the terms proportional to $g'(\eta s)$ and $g'(\eta/s)$ in the third integrand in (B 2) by I_1 and I_2, respectively. Then, (B 2) may be written as

$$\frac{\mathrm{d}U^i_{cl}}{\mathrm{d}\eta} = \int_0^1 s^2K(s)g'(\eta s)\,\mathrm{d}s + \int_0^{\eta/\eta_m} s^3K'(s)g'(\eta s)\,\mathrm{d}s + [I_1]^1_{s=\eta/\eta_m} - [I_2]^1_{s=\eta/\eta_m}. \tag{B 4}$$

Both I_1 and I_2 are singular at $s = 1$; however the singularities cancel each other. As observed earlier, this is consistent with the our interpretation of the original integral in (4.6) as a principal value. For cases where $g(\eta)$ has a singular slope at $\eta = \eta_m$, I_1 is also singular at $s = \eta/\eta_m$ for $\eta \to \eta_m$; this singularity is evidently removed by the second integral which has a singularity at its upper limit that is equal and opposite in sign. The only remaining singularity is therefore that associated with I_2 at $s = \eta/\eta_m$ for $\eta \to \eta_m$. The coefficient of this singularity vanishes when $\lim_{\eta\to\eta_m} g(\eta) \approx (1-\eta/\eta_m)^{1/2}$.

In order to see this, we first evaluate the indefinite integral for $s, \eta/\eta_m \to 1$

$$\lim_{s,\eta/\eta_m\to 1} I_2 = \int \frac{K'(s)}{s^2}\, g'\left(\frac{\eta}{s}\right) \mathrm{d}s$$
$$= -\frac{1}{4}\int \frac{1}{(1-s)(1-\eta/\eta_m s)^{1/2}}\, \mathrm{d}s,$$
$$= -\frac{1}{4}\int \frac{1}{(1-s)(s-\eta/\eta_m)^{1/2}}\, \mathrm{d}s. \tag{B 5}$$

Using $s = 1 - p$ and $\eta/\eta_m = 1 - \hat{\eta}$, we have

$$\lim_{s,\eta/\eta_m\to 1} I_2 = \frac{1}{4}\int \frac{\mathrm{d}p}{p\,(\hat{\eta}-p)^{1/2}}. \tag{B 6}$$

Further, using $p = \hat{\eta}\sin^2\kappa$, we have

$$\lim_{s,\eta/\eta_m\to 1} I_2 = -\frac{1}{2(1-\eta/\eta_m)^{1/2}}\int \frac{\mathrm{d}\kappa}{\sin\kappa}$$
$$= \frac{1}{2(1-\eta/\eta_m)^{1/2}}\ln(\mathrm{cosec}\,\theta - \cot\theta), \tag{B 7}$$

in terms of η with $\theta = \sin^{-1}[(1-s)/(1-\eta/\eta_m)]^{1/2}$. It is immediately seen that $[I_2]_{s=\eta/\eta_m} = 0$. It may, in fact, be shown that with $g(\eta) \approx A(1-\eta/\eta_m)^{1/2}$ for $\eta \to \eta_m$, we have

$$\frac{\mathrm{d}U^i_{cl}}{\mathrm{d}\eta}\,|_{\eta=\eta_m} = \int_0^1 s^2 K(s) g'(\eta_m s)\,\mathrm{d}s + \left[\int_0^{\eta/\eta_m} s^3 K'(s) g'(\eta s)\,\mathrm{d}s + \frac{A}{2(1-\eta/\eta_m)^{\frac{1}{2}}}\ln(1+\sqrt{2})\right], \tag{B 8}$$

where the bracketed term approaches a finite value at $\eta = \eta_m$. According to (4.10), the above, of course, equals 1/3. Again, the non-local nature of the interactions implies that, while being finite, the actual value of $\mathrm{d}U^i_{cl}/\mathrm{d}\eta$ at $\eta = \eta_m$ still depends on the entire number density profile $g(\eta)$ for $\eta \in (0, \eta_m)$. It may be shown that for number density profiles of the form $(1-\eta/\eta_m)^\alpha$ with $0 < \alpha < 1$, all of which satisfy the criterion of a singular slope at $\eta = \eta_m$, the rate of increase of induced velocity diverges as $(1-\eta/\eta_m)^{(\alpha-1)}$ for $\eta \to \eta_m$ with the coefficient of the divergent term changing sign across $\alpha = \frac{1}{2}$; the velocity itself approaches a finite value in all cases. Figure 10 shows plots of the induced velocity for values of α on either side of 0.5, confirming our predictions: for $\alpha > 0.5$ the slope diverges to negative infinity, while for $\alpha < 0.5$ the slope diverges to positive infinity for $\eta \to \eta_m$. In the limit $\alpha \to 0$, the number density approaches a top-hat profile, and the induced velocity itself diverges logarithmically at the rim of the cluster. This divergence arises because, for the discontinuous top-hat profile, the largest contributions to the induced velocity are now of a local nature, stemming from particles located close to the cluster edge, and being given by $\int^{\eta_m} d\eta(1-\eta/\eta_m)^{-1}$.

Appendix C. Limiting form of the non-local contributions to the induced velocity in a planar cluster

As seen in § 4.2, owing to the long-range nature of the inertial hydrodynamic interactions, the contributions to the induced velocity at any point in the cluster from distant regions end up being comparable to those arising from its neighbourhood.

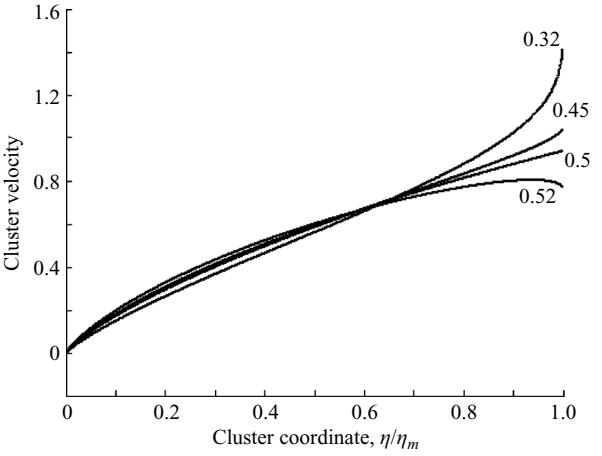

FIGURE 10. The behaviour of the induced velocity for settling clusters of extent η_m with number density profiles of the general form $(1-\eta/\eta_m)^\alpha$; the curves shown are for $\alpha = 0.32, 0.4, 0.5$ and 0.52.

These non-local contributions are characterized, in part, by the term

$$-\int_{\eta/\eta_m}^{1} \mathrm{d}s \left[g\left(\frac{\eta}{s}\right) - g(0) \right] \frac{K'(s)}{s}, \tag{C 1}$$

in (4.13). Herein, we obtain a simplified form of the above term for small η. Thus,

$$-\lim_{\eta \ll 1} \int_{\eta/\eta_m}^{1} \mathrm{d}s \left[g\left(\frac{\eta}{s}\right) - g(0) \right] \frac{K'(s)}{s} \tag{C 2}$$

$$-\lim_{\eta \ll 1} \left[\int_{\eta/\eta_m}^{\eta^\epsilon} \mathrm{d}s \left[g\left(\frac{\eta}{s}\right) - g(0) \right] \frac{K'(s)}{s} - \int_{\eta^\epsilon}^{1} \mathrm{d}s \left[g\left(\frac{\eta}{s}\right) - g(0) \right] \frac{K'(s)}{s} \right], \tag{C 3}$$

where we have introduced a dummy parameter ϵ with $0 < \epsilon < 1$, so that $\eta \ll \eta^\epsilon \ll 1$. One has $(\eta/s) \sim O(1)$ in the first integral, while $(\eta/s) \ll 1$ in the second integral in (C 3). The aim is then to extract an ϵ-independent approximation in the limit $\eta \ll 1$; we expect the first integral to yield an $O(\eta)$ non-local term containing information about $g(\eta)$ for η in the entire range $(0, \eta_m)$, and the second integral to yield an $O(\eta^\alpha)$ local term similar to the second term in (4.13). Using $s = \eta v$ and the small-s asymptote of $K'(s)$ in the first integral, and (4.11) in the second, one obtains

$$\begin{aligned}
&-\lim_{\eta \ll 1} \left[\int_{\eta/\eta_m}^{\eta^\epsilon} \mathrm{d}s \left[g\left(\frac{\eta}{s}\right) - g(0) \right] \frac{K'(s)}{s} - \int_{\eta^\epsilon}^{1} \mathrm{d}s \left[g\left(\frac{\eta}{s}\right) - g(0) \right] \frac{K'(s)}{s} \right] \\
&= -\lim_{\eta \ll 1} \left[\frac{\pi}{4}\, \eta \int_{1/\eta_m}^{1/\eta^{1-\epsilon}} \mathrm{d}v \left[g\left(\frac{1}{v}\right) - g(0) \right] - c\, \eta^\alpha \int_{\eta^\epsilon}^{1} \mathrm{d}s\, \frac{K'(s)}{s^{1+\alpha}} \right] \\
&= \lim_{\eta \ll 1} \left[\frac{\pi}{4}\, \eta \int_{\eta^{1-\epsilon}}^{\eta_m} \mathrm{d}w\, \frac{[g(0) - g(w)]}{w^2} + c\, \eta^\alpha \int_{\eta^\epsilon}^{1} \mathrm{d}s\, \frac{1}{s^{1+\alpha}} \left(K'(s) - \frac{\pi}{4}\, s \right) + c\, \eta^\alpha \int_{\eta^\epsilon}^{1} \mathrm{d}s \frac{\pi}{4 s^\alpha} \right],
\end{aligned} \tag{C 4}$$

where we have used the further change of variables $w = 1/v$ in the first term. On further simplification, (C 4) gives

$$\frac{\pi}{4}\eta\left[\int_0^{\eta_m} \mathrm{d}w \frac{[g(0)-g(w)]}{w^2} - c\int_0^{\eta^{1-\epsilon}} w^{\alpha-2}\mathrm{d}w\right] + c\,\eta^{\alpha}\int_0^1 \mathrm{d}s \frac{1}{s^{1+\alpha}}\left(K'(s) - \frac{\pi}{4}s\right)$$
$$+ c\left[\frac{\pi}{4}\frac{\eta^{\alpha}}{(1-\alpha)} - \frac{\pi}{4}\frac{\eta^{\alpha+\epsilon(1-\alpha)}}{(1-\alpha)}\right] = \frac{\pi}{4}\eta\int_0^{\eta_m} \mathrm{d}w \frac{[g(0)-g(w)]}{w^2} + \frac{\pi}{4}\frac{c\,\eta^{\alpha}}{(1-\alpha)}$$
$$+ c\,\eta^{\alpha}\int_0^1 ds \frac{1}{s^{1+\alpha}}\left(K'(s) - \frac{\pi}{4}s\right), \qquad \text{(C 5)}$$

where the integral involving $K'(s)$ is convergent provided $\alpha < 3$.

REFERENCES

Batchelor, G. K. 1967 *Introduction to Fluid Dynamics* Cambridge University Press, p. 348.

Batchelor, G. K. 1974 Low-Reynolds-number bubbles in fluidized beds. *Arch. Mech.* **26**, 339.

Brady, J. F. & Bossis, G. 1988 Stokesian Dynamics. *Annu. Rev. Fluid Mech.* **20**, 111.

Bretherton, F. P. 1964 Inertial effects on clusters of spheres falling in a viscous fluid. *J. Fluid Mech.* **20**, 401.

Byrd, P. F. & Friedman, M. D. 1971 *Handbook of Elliptic Integrals for Engineers and Scientists.* Springer.

Clift, R., Grace, J. R. & Weber, M. E. 1978 *Bubbles, Drops and Particles.* Academic.

Ekiel-Jezewska, M. L., Metzger, B. & Guazzelli, E. 2006 Spherical cloud of point particles falling in a viscous fluid. *Phys. Fluids* **18**, 038104.

Feng, J., Hu, H. H. & Joseph, D. D. 1994 Direct simulation of initial-value problems for the motion of solid bodies in a Newtonian fluid. Part 1. Sedimentation *J. Fluid Mech.* **261**, 95.

Fortes, A. F., Joseph, D. D. & Lundgren, T. S. 1987 Nonlinear mechanics of fluidization of beds of spherical particles. *J. Fluid Mech.* **177**, 467.

Gadala-Maria, F. & Acrivos, A. 1980 Shear-induced structure in a concentrated suspension of solid spheres. *J. Rheol* **24**, 799.

Gakhov, F. D. 1966 *Boundary Value Problems* Pergamon.

Gradshteyn, I. S. & Ryzhik, I. M. 1965 *Table of Integrals, Series and Products.* Academic.

Happel, J. & Brenner, H. 1973 *Low Reynolds Number Hydrodynamics.* Noordhoff.

Hocking, L. M. 1964 The behavior of clusters of spheres falling in a viscous fluid. Part 2. Slow motion theory. *J. Fluid Mech.* **20**, 129.

Hogg, A. J., Hallworth, M. A. & Huppert, H. E. 2005 On gravity currents driven by constant fluxes of saline and particle-laden fluid in the presence of a uniform flow. *J. Fluid Mech.* **539**, 349.

Hogg, A. J., Ungarish, M. & Huppert, H. E. 2001 Effects of particle sedimentation and rotation on axisymmetric gravity currents. *Phys. Fluids* **13**, 3687.

Hu, H. H., Joseph, D. D. & Crochet, M. J. 1992 Direct simulation of fluid particle motions. *Theor. Comput. Fluid Dyn.* **3**, 285.

Jayaweera, K. O. L. F., Mason, B. J. & Slack, G. W. 1964 The behavior of clusters of spheres falling in a viscous fluid. Part 1. Experiment. *J. Fluid Mech.* **20**, 121.

Kim, S. & Karrila, S. J. 1991 *Microhydrodynamics: Principles and Selected Applications.* Butterworth-Heinemann.

Koch, D. L. 1993 Hydrodynamic diffusion in dilute sedimenting suspensions at moderate Reynolds numbers. *Phys. Fluids* A **5**, 1141.

Koch, D. L. & Hill, R. J. 2001 Inertial effects in suspension and porous-media flows. *Annu. Rev. Fluid Mech.* **33**, 619.

Kojima, M., Hinch, E. J. & Acrivos, A. 1984 The formation and expansion of a toroidal drop moving in a viscous fluid. *Phys. Fluids* **27**, 19.

Leshansky, A. M., Lavrenteva, O. M. & Nir, A. 2003 The weakly inertial settling of particles in a viscous fluid. *Proc. R. Soc. Lond.* A **459**, 3079.

Machu, G., Walter, M., Nitsche, L. C. & Schaflinger, U. W. E. 2001 Coalescence, torus formation and breakup of sedimenting drops: experiments and computer simulations. *J. Fluid Mech.* **447**, 299.

Metzger, B., Nicolas, M. & Guazzelli, E. 2007 Falling clouds of particles in viscous fluids. *J. Fluid Mech.* **580**, 283.

Muskhelishvili, N. I. 1992 *Singular Integral equations*. Dover.

Nicolas, M. 2002 Experimental study of gravity-driven dense suspension jets. *Phys. Fluids* **14**, 3570.

Nitsche, J. M. & Batchelor, G. K. 1997 Break-up of a falling drop containing dispersed particles. *J. Fluid Mech.* **340**, 161.

Vasseur, P. & Cox, R. G. 1977 The lateral migration of spherical particles sedimenting in a stagnant bounded fluid. *J. Fluid Mech* **80**, 561.

Yin, X. & Koch, D. L. 2007 Hindered settling velocity and microstructure in suspensions of spheres with moderate Reynolds number. *Phys. Fluids* **19**, 093302.